A novel mouse model reproducing frontal alterations related to the prodromal stage of dementia with LEWY bodies

Estelle Schueller, Iris Grgurina, Brigitte Cosquer, Elodie Panzer, Noémie Penaud, Anne Pereira de Vasconcelos, Aline Stéphan, Karine Merienne, Jean-Christophe Cassel, Chantal Mathis, et al.

Neurobiology of Disease 201 (2024) 106676

Contents lists available at ScienceDirect

Neurobiology of Disease

journal homepage: www.elsevier.com/locate/ynbdi

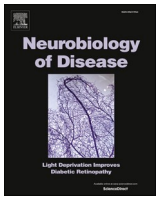

A novel mouse model reproducing frontal alterations related to the prodromal stage of dementia with LEWY bodies

Estelle Schueller [a,1], Iris Grgurina [a,1], Brigitte Cosquer [a], Elodie Panzer [a], Noémie Penaud [a], Anne Pereira de Vasconcelos [a], Aline Stéphan [a], Karine Merienne [a], Jean-Christophe Cassel [a], Chantal Mathis [a], Frédéric Blanc [b,c], Olivier Bousiges [a,b,d,*], Anne-Laurence Boutillier [a,*]

[a] Université de Strasbourg, Laboratoire de Neurosciences Cognitives et Adaptatives (LNCA), UMR7364 CNRS, 12 Rue Goethe, Strasbourg, France
[b] ICube Laboratory UMR 7357 and FMTS (Fédération de Médecine Translationnelle de Strasbourg), IMIS team, University of Strasbourg and CNRS, Strasbourg, France
[c] CM2R (Research and Resources Memory Center), Geriatric Day Hospital, Neurogeriatric Service, Geriatrics Department, University Hospital of Strasbourg, Strasbourg, France
[d] University Hospital of Strasbourg, Laboratory of Biochemistry and Molecular Biology, Avenue Molière, Hôpital de Hautepierre, Strasbourg, France

ARTICLE INFO

Keywords:
Dementia with Lewy bodies
Transgenic mouse model
α-Synuclein
Prodromal stage
Human cohort
Frontal cortex

ABSTRACT

Background: Dementia with Lewy bodies (DLB) is the second most common age-related neurocognitive pathology after Alzheimer's disease. Animal models characterizing this disease are lacking and their development would ameliorate both the understanding of neuropathological mechanisms underlying DLB as well as the efficacy of pre-clinical studies tackling this disease.
Methods: We performed extensive phenotypic characterization of a transgenic mouse model overexpressing, most prominently in the dorsal hippocampus (DH) and frontal cortex (FC), wild-type form of the human α-synuclein gene (mThy1-hSNCA, 12 to 14-month-old males). Moreover, we drew a comparison of our mouse model results to DH- and FC- dependent neuropsychological and neuropathological deficits observed in a cohort of patients including 34 healthy control subjects and 55 prodromal-DLB patients (males and females).
Results: Our study revealed an increase of pathological form of soluble α-synuclein, mainly in the FC and DH of the mThy1-hSNCA model. However, functional impairment as well as increase in transcripts of inflammatory markers and decrease in plasticity-relevant protein level were exclusive to the FC. Furthermore, we did not observe pathophysiological or Tyrosine Hydroxylase alterations in the striatum or substantia nigra, nor motor deficits in our model. Interestingly, the results stemming from the cohort of prodromal DLB patients also demonstrated functional deficits emanating from FC alterations, along with preservation of those usually related to DH dysfunctions.
Conclusions: This study demonstrates that pathophysiological impairment of the FC with concomitant DH preservation is observed at an early stage of DLB, and that the mThy1-hSNCA mouse model parallels some markers of this pathology.

1. Introduction

Dementia with Lewy bodies (DLB) is the second most common neurodegenerative pathology after Alzheimer's disease (AD) (Zaccai et al., 2005). Rather early in disease development, both DLB and AD patients display cognitive deficits, affecting episodic, working memory or/and executive functions. Due to the plethora of shared symptoms, particularly in prodromal stages of the disease, differential diagnosis between AD and DLB remains challenging (Nelson et al., 2010). Besides, DLB is a pathology close to Parkinson's disease (PD) due to the presence

Abbreviations: DLB, Dementia with Lewy bodies; AD, Alzheimer's disease; PD, Parkinson's disease; PDD, Parkinson's disease dementia; MSA, Multiple system atrophy; α-syn, α-synuclein; Thy1, Thymus cell antigen; FC, frontal cortex; DH, dorsal hippocampus; Str, striatum; pSyn129, phosphorylated α-synuclein at serine 129; RL/RI-16, Free and Cued Selective Reminding Test; DMS-48, The Delayed Matching to Sample test-48 items; FAB, The Frontal Assessment Battery.

* Corresponding authors at: Laboratoire de Neurosciences Cognitives et Adaptatives (LNCA UMR Université de Strasbourg /CNRS 7364), 12 Rue Goethe, 67000 Strasbourg, France.
E-mail addresses: bousiges@unistra.fr (O. Bousiges), laurette@unistra.fr (A.-L. Boutillier).
[1] Equal contribution

https://doi.org/10.1016/j.nbd.2024.106676
Received 14 February 2024; Received in revised form 20 August 2024; Accepted 18 September 2024
Available online 20 September 2024

of parkinsonism (bradykinesia, rigidity, postural instability, and resting tremor), that remains discrete or absent at the prodromal stage (McKeith et al., 1996; Donaghy and McKeith, 2014). Another feature common to DLB and PD is their neuropathophysiology, characterized by the presence of neuronal α-synuclein (α-syn) aggregates in form of Lewy bodies and Lewy neurites (Spillantini et al., 1997). However, while in PD α-syn aggregates are mostly localized in the brainstem and substantia nigra, in DLB they are rather diffuse throughout the entire brain as of the prodromal stage. Moreover, PD and DLB, alongside with Parkinson's disease dementia (PDD) and multiple system atrophy (MSA), make up α-synucleinopathies, a group of neurodegenerative diseases characterized by the abnormal accumulation of α-syn in the brain. The interchangeability of symptoms between DLB and the aforementioned diseases imposed a substantial challenge to its correct diagnosis, resulting in unrecognition of DLB as a full-fledged neuropathology per se until 1996 (McKeith et al., 1996). These diagnostical difficulties are accentuated in early stages when there is amplified symptomatic vagueness and heterogeneity among DLB probable subjects. Hence, to this moment there is no operationalized diagnostic criteria for prodromal DLB, with mild cognitive impairment being its sole acknowledged prodrome due to its easier testability as compared to delirium- and psychiatric-onset presentations, which are also proposed as early DLB manifestations (McKeith et al., 2020).

Various transgenic animal models with altered α-syn expression have been developed thus far, largely prompted by the fact that patients with familial forms of PD carry mutated or overexpressed (duplication or triplication) forms of the *SNCA* gene. However, the vast majority of these models are suitable solely for PD-related studies since they are predominantly over-expressing α-syn in the substantia nigra and/or striatal regions - resulting in immediate and prevalent motor deficits not common for DLB at early stages (Crabtree and Zhang, 2012; Outeiro et al., 2019). It should be noted that some studies have also examined cognitive, and not only motor deficits present in PD models (Hatami and Chesselet, 2015). Their observations, however, are not eligible for extrapolation in the context of pure DLB, especially in its early state where motor symptoms are mild to non-existent.

The objective of the current study was to phenotype a novel murine model of α-synucleinopathy, overexpressing the wild-type form of human α-syn gene under the neuron-specific murine thymus cell antigen 1 (Thy-1) promoter (Thy1hSNCA, Jackson Laboratories), for its potential to mimic DLB-specific pathology. Since these mice display notably elevated α-syn expression in the frontal cortex (FC) and dorsal hippocampus (DH), structures highly involved in cognitive functions and affected in DLB cases (Outeiro et al., 2019; Blanc et al., 2015, 2016; Oppedal et al., 2019), we aimed to assess their associated molecular, anatomopathological and cognitive deficits. Moreover, we hypothesized that due to the prevalence of α-syn expression in these structures, as compared to previous models whose predominant structures of expression were of striatal origin, the mThy1-hSNCA model could potentially provide for the currently missing model of DLB.

2. Materials and methods

2.1. Animal care

Animal care and experimental protocols were in accordance with the institutional guidelines and directive 2010/63/EU on the protection of animals used for scientific purposes (European parliament and council, September 22, 2010). Protocols have been approved by the CREMEAS, ethics committee of Strasbourg, France (APAFIS #406). The mThy1-hSNCA hemizygous mice (SNCA mice) were obtained from the Jackson Laboratory (C57BL/6 N-*Slc4a7*$^{Tg\ (Thy1\text{-}SNCA)12Mjff}$/J, stock No 016936; Ouyang, 2011) and were backcrossed and bred with C56BL/6 J females upon arrival to our facility. The SNCA transgenic mice overexpress human WT α-synuclein (*SNCA*) gene under the control of the murine thymus cell antigen 1 (mThy1) promoter, allowing for neuron-specific transgene expression throughout the brain. The expression was reported as being relatively high in the cerebral cortex and hippocampus, while relatively low in the kidney (Jackson Laboratory). The model has not been previously phenotyped. Their littermates lacking the human SNCA expression were used as respective controls and are referred to as WT or control throughout the rest of the article. The animals were housed in a temperature- and hygrometry-controlled room on a 12-h light/dark cycle with food and water ad libitum. They were individually housed one week prior to behavioral testing, which were conducted during the light phase of their cycle. Behavioral characterization and RT-qPCR analyses were performed on 12–14-month-old SNCA males, with WT littermates serving as a control. Protein quantification, as well as histological studies, were performed on brain samples from 14-month-old male SNCA and WT mice.

2.2. Animal handling

Mice were handled by the experimenter prior to behavioral testing. Since testing episodic-like memory using objects is a sensitive task, mice were not handled directly by the tail but rather by tube. Therefore, one week before the test, one tube was placed into each cage and during the three days preceding the task mice were habituated, twice a day to transportation by tube. Given that mice spontaneously enter the tube, allows the experimenter to avoid any direct handling. However, for the Morris Water Maze (MWM) task, due to the nature of the test, mice were handled by the tail. Testing subjects were placed in the room where the behavioral study was taking place 30 min before the start of the study.

2.3. Episodic-like memory tasks using objects

The apparatus used for these tests was an open field made of opaque black plexiglass (55 × 55 × 40 cm). The objects to be discriminated were made of glass, plastic or metal and existed in duplicate. The mice were not able to displace them. For each day of the test, pairs or trio of objects differed, as well as their localization in the open field. There was a constant illumination of 15 lx in the middle of the apparatus and background noise of 50 dB. The episodic-like memory tasks were based on rodent's spontaneous tendency to preferentially explore a new object (novel object recognition), a familiar object displaced to a new location (object location), or a familiar object in a location previously occupied by a different object (object-in-place). Each mouse was tested for 4 days, starting with habituation. During the habituation phase mice received two 10-min trials, with 3 h delay in between them, not changing the objects localization between the trials. On days 2 and 3 mice were tested for novel object recognition (NOR) and object location (OL) memory. Here, the mice received one sample trial in which they were left to explore the objects for 10 min, followed by a 10-min test trial 3 h later. Between sample and test trials one object was either replaced by an unfamiliar one (NOR) or it was displaced (OL). On day 4 the mice performed the object-in-place (OiP) task in which sample and test trials were 15 min long and 5 min apart. Two non-identical objects were presented during the sample trial, with one being replaced by a duplicate of the other during the test trial. Between sample and test trials, mice were consistently returned to their homecage. Exploration time was followed with a stopwatch and was determined as time during which the mice's nose was directed towards the object less than 2 cm from it. Biting, running around or climbing on the objects was not considered as exploration.

2.4. Spatial reference memory task using the Morris water maze

This task is based on mice's aversion to cold water (21 °C ± 1 °C) from which stems their motivation to stay in it for as short a time as possible. Mice had to locate a hidden platform submerged in opaque water using surrounding environmental spatial cues. The apparatus used was a circular tank with a diameter of 146 cm and a height of 60 cm that

can be virtually separated into 4 equal quadrants (South-East (SE), South-West (SW), North-West (NW), North-East (NE)), and that is filled with opacified water at 21 °C. During the 1-min per animal habituation trial, that is preceding the spatial learning phase, a visible platform was placed in the NW quadrant, emerging from the water over 1 cm. At this phase the depth of the water was of 5 cm. If the mice did not reach the platform by themselves before the end of the habituation trial, the experimenter guide them to it. On the second day, the 120 s forced swim trial was conducted and the platform was removed to habituate the mouse to swimming but also to the fact that the platform was now invisible during the test. This step also allowed the experimenter to verify whether there was a spontaneous predilection for a particular quadrant. During the following 5-days of acquisition, a hydraulic platform with a 10 cm diameter was placed in the SE quadrant 1 cm below the water level; now the depth of water was of 40 cm, rendering the platform invisible. The room was highly contrasted so that the mice could use distal visual cues. A camera attached above the water maze enabled recording of behavior by an automated animal tracking system (Any-Maze, UgoBasile). The spatial learning phase lasted for 5 days with 4 discrete trials each day. The mice were placed into the water facing the wall of the maze, with different starting points from trial to trial in order to promote spatial learning. The trial ended when the mouse had reached the hidden platform or, if after 60s the mice did not find the platform by themselves, when the experimenter had guided them to it. Whatever the way by which the mice reached the platform, they were left on it for 15 s. The platform was never displaced during learning. "Recent" long term memory was tested 24 h after the fourth day of learning and followed by the fifth acquisition to avoid memory extinction. "Remote" long term memory was tested 21 days after the fifth and last day of learning. During each of these probe trials, the platform was lowered, disabling the mice to reach it. When the mice remembered the platform location, they spent more time in the target quadrant than by chance (15 s).

2.5. Locomotor activity

The actigraphy test consisted of recording the animal's spontaneous locomotor activity in the homecage over day- and nighttime intervals (12-h light/dark cycle in housing facility). The cages were placed on an actigraphy rack with photoelectric cells emitting infrared beams at each extremity of the cage. This apparatus was connected to a computer with a software recording infrared beam crossings. Successive crossing of the two beams was considered as a horizontal travel, reflecting mice's locomotor activity. Mice were housed in individual cages (29,5 × 11,5 × 13 cm) with both clean and a small portion of their own homecage bedding. The thickness of bedding was limited to avoid possible disruption of the infrared beams. The cages were placed on the rack and the locomotor activity was recorded over two nights and two days, at a 10 min acquisition frequency.

2.6. Nesting or nest-building

Nest-building is a spontaneous daily activity for mice, even under laboratory housing conditions, since the nests provide thermoregulation and sanctuary from light and humans. In this study, we chose to assess nest-building because it can be paralleled with activity of daily living (ADL) in humans (Jirkof, 2014). It is important to keep in mind that motor dysfunctions or depressive-like phenotype can alter the nesting capacity. For testing, each mouse was placed in a clean cage (32 × 16 × 14 cm) with 6 pieces of paper, usually used for building the nest, displaced in each corner and against the longer walls of the cage. The test was performed in the housing facility. Two scores were attributed to each mouse at three time points (1 h40 min, 3 h, 24 h): 1/ "zone score" ranging from 0 to 5 scored according to whether a piece of paper was or not in a given zone and 2/ "quality score" ranging from 0 to 20. The quality score was attributed following Gaskill and colleagues' protocol (Gaskill et al., 2013).

2.7. Buried food

This test was used to assess mice's olfaction by measuring the time spent finding a familiar palatable food in the cage, hidden 2 cm under clean bedding (32 × 16 × 14 cm). The protocol used is adapted from Yang and Crawley (Yang and Crawley, 2009). For two days preceding the test, a new palatable food (CHOCAPIC®, Nestlé Céréales) was introduced in the homecage setting for each mouse. The following morning it was checked if the mice had eaten the introduced food or not (not eating indicating the foods lack of palatability). On the day of the test each mouse was placed in a new cage with clean bedding, away from the buried palatable food. The time spent to find the food was measured for each mouse, and a mean was calculated for each experimental group.

2.8. Novel taste learning

This test was based on rodent's neophobia towards new food. Mice were accustomed to eating only a small portion of the new food, as means of checking its quality. If they showed the food was palatable to them, they usually prefer this food upon subsequent presentation. We used lucerne nibble sticks for rodents (McGreen®, Vitakraft®) as new food. The protocol was adapted from Swank and Sweatt (Swank and Sweatt, 2001). Both WT and SNCA mice were separated in two groups: naive, not familiar with the food before the test, and pre-exposed one, which received the new food 3 days prior to testing. Throughout those three days, the pre-exposed mice receive half a stick of lucerne and the morning following the third day we checked if there was any food left. The 2 following days none of the groups received the new food and on the third one each mouse received half a stick of lucerne, which had been weighed before. After 10 min, the food was removed and weighed to measure the quantity that was eaten (mg) per mouse. A mean was calculated for each group. The hypothesis for this test is that the pre-exposed group will eat more, compared to the naive one.

2.9. Beam crossing test

This test was used to assess sensorimotor function, more specifically motor coordination, and was performed according to Fleming and colleagues' protocol (Fleming et al., 2013) with the exception that our apparatus was a simple wooden bar (1 cm large x 80 cm long) with a platform at the extremity that the mice had to reach. The time spent to cross the bar from the extremity to the platform was recorded using a stopwatch during the 5 trials on the test day. The trials were recorded, and the errors (limb slips) were assessed by watching the videos in slow motion. The mean scores of beam's crossing and errors were calculated for each group.

2.10. Protein preparation

Brains were collected from 14-month-old male mice, killed by cervical dislocation, and structures of interest were dissected on ice (frontal cortex (FC), striatum (Str), dorsal hippocampus (DH), cerebellum (Cb)). The tissue was collected in 1.5 ml tubes and immediately frozen in liquid nitrogen, at −80 °C, where it was stored until use. Tissues were lysed and homogenized in 4× Laemmli buffer (Bio-rad, #1610747), with addition of 1/10 β-mercaptoethanol (Sigma-Aldrich, #444203), and mixed with sample to obtain a final 1× solution. After sonication (2 × 10 s, amplitude 40 %), 10 min at 70 °C and 5 min at 100 °C heating, samples were centrifuged (14,000 *g* for 5 min) and the supernatant was frozen at −20 °C until use. Protein concentration was measured using the Qubit™

Protein Assay Kit (ThermoFisher Scientific, #Q33211). To separate Triton-soluble and -insoluble fractions, a protocol adapted from Zhou et al. (2008) was used. Briefly, tissue samples from 12-month-old male mice were lyzed into 150 µl of dissociation buffer (50 mM Tris pH 7.4, 10 mM NaCl, 1 mM EDTA, 1 % Triton X-100 complemented with protease inhibitor cocktail 1/100) with a dounce homogenizer. Samples were left on ice for 30 min and centrifuged at 14000 *g*, 4 °C during 20 min. Supernatants were kept as the triton-soluble fraction (SF). Pellets representing the triton-insoluble fraction (IF) were further dissociated in 4× SDS Laemmli Buffer, followed by sonication (2× 10s, amplitude 40 %) and centrigugation at 14000 *g* for 20 min. The supernatants were recovered as SDS-soluble fractions. All samples (SF and IF) were adjusted to 1× Laemmli Buffer, heated 10 min at 70 °C, 5 min at 100 °C, and centrifuged (14,000 *g*, 5 min). Protein concentrations of supernatants were measured using the RG-DC Protein Assay Kit from Biorad (#5000119).

2.11. Western blot

Western blots were performed as described previously (Chatterjee et al., 2018) with antibodies against total α-syn (Santa Cruz, #SC-7011R), α-syn phosphorylated on serine 129 (pS129) (Abcam, #Ab51253), murine specific α-synuclein (Cell Signaling, # D37A6), neuronal nucleus (NeuN) (Millipore, #ABN78), α-tubulin (Sigma-Aldrich – 05-829), glial fibrillary acidic protein (GFAP) (Millipore, #MAB360), synaptophysin I (Syp I) (Synaptic System, #101011), PSD95 (Santa Cruz, #SC-32290), neurogranin (Nrgn) (Santa Cruz, #SC-50401) and Rab10 (Abcam, #Ab237703). Secondary HRP-conjugated antibodies directed against mouse, rabbit, or rat were from Jackson ImmunoResearch. If the membrane was stripped and reprobed it was done by incubating it in the stripping buffer (20 % of 10 % SDS, 12.5 % Tris base 0,5 M pH = 6,8, 0.8 % of β-mercaptoethanol and 67 % dH20) for 20 min in a water bath (70 °C), followed by 3 × 5-min washes (TBST buffer) to remove primary and secondary antibodies bound to the membrane. Molecular weight marker used was PageRulerTM Plus Prestained Protein, 26,619, Thermo Scientific). Blots were revealed using an Electro chimioluminescence kit (ECL) (Bio-Rad, #1705060) and visualized in a ChemiDoc molecular imager (Bio-Rad). Results were quantified using ImageLab software (Bio-Rad). All blots were performed using stain-free gels, for which protein level quantifications were normalized to total protein levels transferred onto the nitrocellulose (see Supplemental raw blot images), except those of murine α-synuclein and α-tubulin, for which murine α-synuclein levels were normalized to α-tubulin loading control.

2.12. Tissue preparation for immunohistochemistry

Mice were killed when aged of 14 months by intraperitoneal injection of sodium pentobarbital (182,2 mg/kg, Doléthal®, Vetoquinol) that was followed by transcardial perfusion with cold NaCl (0,1 % during 3 min) and PFA (4 % during 8 min). Fixed brains were harvested, post-fixed in PFA (4 % for 2 h), and cryoprotected during 48 h in a 20 % sucrose solution. Finally, brains were snap frozen by 1 min long immersion in isopentane at −35 °C and kept at −80 °C until use. Free floating, 30 µm thick frontal brain sections were prepared using a frozen microtome (Microm HM560, Thermo Scientific). The slices were kept in a cryoprotection solution at −20 °C until use.

2.13. Cresyl violet staining

Cresyl violet is a basic compound binding to acid macromolecules (i.e., DNA and RNA), thus staining the nucleus and cytoplasm of neuronal and glial cells in dark blue/purple. Neuronal cytoplasm is more abundant in RNA than glial cells, so neurons appear darker than glia, which appear light blue. Frozen brain sections (30 µm) from DH were washed in 1× PBS (3 × 10 min), mounted on glass slides, and left to dry overnight. The following day they were washed in distilled water (3 × 3 min) and stained with 0,5 % cresyl violet solution at 55 °C for 9 min. This was followed by wash in distilled water (3 × 3 min), and two increasing degree ethanol baths (70 °C for 3 min, 95 °C for 2 min), one 20 s bath in alcohol/acid for bleaching, and then again three increasing degree ethanol baths (95 °C for 4 min, 2 × 100 °C for 4 min each). Finally, the slides were put in a xylene bath for 5 min, before mounting with EUKITT® medium for microscopic image analysis (Leica DM5500B). Measures of cellular layers' thickness (CA1, CA3, DG ventral and dorsal parts) were performed with FIJI software (Image J). The mean thickness was calculated on three distinct levels of antero-posteriority (AP_1 = −1,58 mm, AP_2 = −1,94 mm, AP_3 = −2,30 mm) per animal (n = 3 WT + 3 SNCA).

2.14. Immunohistochemistry

DAB staining: To identify α-syn pathology, immunohistochemistry against α-syn pS129 was realized on floating sections (n = 3 WT + 4 SNCA). All steps were at room temperature under slow agitation. After rinsing in PBS 1× (3 × 10 min), sections were placed in 1 % hydrogen peroxide for 10 min to inhibit endogenous peroxidases. Blocking of unspecific sites and permeabilization were realized by incubating the sections with 5 % goat serum in 0,5 % TritonX-100 diluted in PBS 1× for 30 min. The brain sections were incubated overnight with anti-α-syn pS129 antibody (Ab51253, Abcam) diluted at 1/2000 in 5 % goat serum and 0,05 % Triton X-100 PBS solution. After washing, slices were further incubated with an anti-rabbit antibody (ZB-1007, Vector Laboratories) for 1 h, diluted at 1/500 in the same solution as the primary antibody. Staining amplification using avidin-biotin-peroxidase complex (ABC Vectastain kit, PK-6100, Vector Laboratories) was realized for 45 min, and after washing with PBS and TRIS buffers the staining was revealed by incubation in 3,3′-diaminobenzidine (DAB) (DAB kit, SK-4100, Vector Laboratories) for 8 to 10 min. Finally, the brain sections were washed, mounted on glass slides, dried overnight at room temperature and mounted in Diamount (030400 A, Diapath) for observation. Acquisitions were performed at 40 x magnification using a digital slide scanner (Nanozoomer S60, Hamamatsu).

Immunofluorescent stainings were performed using standard protocol as described (Chatterjee et al., 2018) using GFAP (Rabbit mAb #173008, Synaptic System;1/2000), Iba1 (Guinea pig mAb #234308, Synaptic System;1/1000) and Tyrosine Hydroxylase (TH) (Rabbit mAb #58844, E2L6M, Cell Signaling;1/1000) antibodies. Secondary antiobodies used were Goat anti-guineapig Alexa Fluor® 594 AffiniPure (#A11076, Invitrogen, 1:2000), Donkey anti-rabbit Alexa Fluor® 488 (#A21206, Invitrogen, 1:2000), Donkey anti-rabbit Alexa Fluor® 594 (#A21207, Invitrogen, 1:2000) and DAPI nuclear staining was performed (Thermo Fisher Scientific, #62248; 1:10000). Sections were mounted using Mowiol (Millipore, # 475904). Image acquisitions for GFAP and Iba1 were performed at 40 x magnification using a digital slide scanner (Nanozoomer S60, Hamamatsu). Observation and image acquisitions for TH were performed using a fluorescence microscope (Zeiss). IHC quantifications of intensities and densities were performed using QPath.

2.15. ThioflavinS staining

For the ThioflavinS staining 30 µm thick mouse sections of 12-month-old SNCA and 8-month-old THY-Tau22 males (FC and DH) were washed in PBS (3×, 10 min), mounted on slides and left to dry overnight. THY-Tau22 mice are a model of tau aggregation (https://www.alzforum.org/research-models/thy-tau22#:~:text=THY%2DTau22%20mice%20are%20a,tau%20inclusions%2C%20and%

Table 1
Clinical and demographic characteristics of patients.

	Healthy controls $N = 34$	Pro-DLB $N = 55$	Statistical test, P	Post hoc[e]
Age, years [a]	66.5 (8.7)	68.7 (9.4)	U = 804.5 $P = 0.272$	
Gender (F/M)	19/15	30/25	$\chi2 = 0.015$, $P = 0.902$	
MMSE score [b]	28.8 (1.2) (1ND)	28.0 (1.2)	U = 584.5 $P = 0.0038$	HC > Pro-DLB
Years of education	13.0 (3.3) (2ND)	12.2 (3.7) (4ND)	U = 692 $P = 0.246$	
Hallucinations[c]	16.7 % (4 ND)	74.5 %	$\chi2 = 26.19$, P < 0.0001	Pro-DLB > HC
Fluctuations[c]	3.0 % (1 ND)	57.4 % (1 ND)	$\chi2 = 26.05$, $P < 0.0001$	Pro-DLB > HC
Parkinsonism				
Rigidity 0/1/2/3/4	31/1/0/0/ 0 (2 ND)	18/31/3/1/ 0 (2 ND)	U = 312.2 P < 0.0001	Pro-DLB > HC
Akinesia 0/1/2/3/4	31/1/0/0/ 0 (2 ND)	22/28/3/0/ 0 (2 ND)	U = 377 P < 0.0001	Pro-DLB > HC
Tremor at rest 0/1/2/3/4	31/1/0/0/ 0 (2 ND)	37/15/0/0/ 0 (3 ND)	U = 644 P < 0.0001	Pro-DLB > HC
RBD[c]	36.4 % (1ND)	61.1 % (1 ND)	$\chi2 = 5.02$, $P = 0.025$	Pro-DLB > HC
FCSRT[d]	8.8 %	10.9 %	$\chi2 = 0.101$,	
Free recall score	30.0 (5.5) 46.06 (2.9)	24.9 (7.1) 44.3 (5.1)	$P = 0.751$ $t = 3.587$	HC > Pro-DLB
Total recall score			$P = 0.0006$ U = 678 P = 0.026	HC > Pro-DLB
FAB	17.2 (1.1) (2ND)	15.6 (2.2) (7ND)	U = 415.5 $P = 0.0003$	HC > Pro-DLB
DMS48				
Immediate recognition	47.0 (1.4) 47.1 (1.0)	44.8 (4.2) (1ND)	U = 548 P = 0.001	HC > Pro-DLB
Delayed recognition		44.7 (3.8) (3ND)	U = 574 $P = 0.0045$	HC > Pro-DLB

MMSE = Mini-Mental Status Examination; N = number; ND = not done, RBD = Rapid Eye Movement sleep Behavior Disorder; FCSRT = Free and Cued Selective Reminding Test, FAB = Frontal Assessment Battery, DMS48 = Delayed Matching to Sample test-48 items.

[a] Age at time of cognitive evaluation and diagnosis. Mean (standard deviation).

[b] Mean (standard deviation).

[c] Percentage.

[d] percentage of deficient patients.

[e] Mann-Whitney (U), Unpaired t-test (t).

20ghost%20tangles.) The protocol was adapted from Ising et al. (2019). They were then incubated with 0.1 % Sudan Black in 70 % ethanol for 20 min to quench autofluorescence, and extensively washed with PBS. The quenching was followed by a 5 min incubation with 0.025 % thioflavin S (Sigma) in 50 % ethanol (RT, no light), quick washes in 50 % ethanol (2× for 2 min) and longer washing steps in water (2× for 5 min). Stained sections were stored in the dark (4 °C) while observation and image acquisition were performed using a fluorescent microscope (Zeiss).

2.16. RNA-isolation and RT-qPCR

FC and DH of 12–14-month-old mice were harvested and snap-frozen in liquid nitrogen until use. Frozen tissues were homogenized using 1 ml of QIAzol Lysis Reagent (Qiagen, #79306) with a tissue grinding pestle and total RNA was isolated using RNeasy Lipid Tissue Mini Kit (Qiagen; Cat # 74804) following the manufacturer's instructions. cDNA was synthetized from 300 ng of total RNA using the Maxima First Strand cDNA Synthesis Kit (Thermo Scientific, #K1641) under manufacturer's recommended conditions. Real-time PCR was carried out on the T100 Thermal cycler (Bio-Rad) using the PowerUP SYBR Green Master Mix (Applied Biosystems, #A25741), data were analyzed using the 2-DDCT method (Livak and Schmittgen, 2001). and normalized to both *Polr2a* and *36b4* housekeeping gene levels. Values are expressed as relative to control, which is set at 1.

List of the oligonucleotides used in the study (Eurogentec):

Gene name	Forward primer (5′ → 3′)	Reverse primer (5′ → 3′)
SNCA	TTGCAGCAGCCACTGGCTTTG	GCTCCCTCCACTGTCTTC
Snca	GGAGTGACAACAGTGGCT	GCTCCCTCCACTGTCTTC
Rplp0	ACTTACTGAAAAGGTCAAGGC	TCCTCATCTGATTCCTCCGA
Polr2	AATCCGCATCATGAACAGTG	TCATCCATTTTATCCACCACC
Gfap	CGCGAACAGGAAGAGCGCCA	GTGGCGGGCCATCTCCTCCT
Dlg4	CCCCTACCCCTCCTGAGAAT	CCCCTACCCCTCCTGAGAAT
Rab10	TGAGAACATCAGCAAGTGGC	CATGCTCCCTTGCAATCTGT
Syp	TTATCAACCCGATTACGGGC	TGGGCTTCACTGACCAGATT
C1qa	TGAAACTTGGCAGTGTCCTG	TCTCCATGGTGTCCCTGC
Il1b	AAGCTTCCTTGTGCAAGTGT	ATCTTTTGGGGTCCGTCAAC
Cd68	GACCTACATCAGAGCCCGAGT	CGCCATGAATGTCCACTG
Tnf	TCTCATCAGTTCTATGGCCC	GGGAGTAGACAAGGTACAAC
Ifngr2	GAAACAACAGCAAATGCCTCC	GTACTTCACTCGGCTTTGGT
Aif1	GTACTTCACTCGGCTTTGGT	GGAATTGCTTGTTGATCCCC
Tgfb1	GCAACAATTCCTGGCGTTAC	CCTGTATTCCGTCTCCTTGG
Ccl4	GCCCTCTCTCTCTCCTCTTGCT	GAGGGTCAGAGCCCATTG
C3	GAAGGATGGACAAAGCTGGT	AGGCCTTTATGCAGTTCTCG
Il6	GTTCTCTGGGAAATCGTGGA	TGTACTCCAGGTAGCTATGG
Itgax	TGTACTCCAGGTAGCTATGG	TGTACTCCAGGTAGCTATGG

2.17. Neuropsychological tests of the human cohort

55 prodromal DLB (Pro-DLB) patients and 34 healthy controls (HCs) were enrolled in the present study (AlphaLewyMA cohort registered in ClinicalTrials.gov: https://clinicaltrials.gov/ct2/show/NCT01876459). Ethics approval and consent to participate: CPP Est IV, Eudract 2012-A00992–41 / HUS 5330.

Table 1 summarizes the main clinical information of the patients included in the present study. Patients were recruited from the tertiary Memory Clinic (CM2R) of Strasbourg University Hospital, France. Healthy elderly Controls (HC) were recruited among patient's friends and relatives or among participants attending the hospital's Clinical Investigation Center (CIC). Pro-DLB were defined as patients having MCI with probable DLB (i.e., two core symptoms) according McKeith's criteria (McKeith et al., 2020). Fluctuations were assessed with the Mayo Clinic Fluctuations Scale (Ferman et al., 2004). The Hallucinations Parkinson's disease-associated psychotic symptoms questionnaire was used to evaluate the presence of hallucinations (Fenelon et al., 2010). Rapid eye movement (REM) sleep behavior disorder (RBD) was evaluated using a questionnaire based on the article by Gjerstad et al., 2008 (Gjerstad et al., 2008), simplified into two questions for the patient and the caregiver, one concerning movements during sleep and the other concerning vivid dreams and nightmares.

To assess specific cognitive domains, we used the following neuropsychological tests: ***Sixteen (16)-item Free and Cued Recall***, which is the French version of the Free and Cued Selective Reminding Test (*Rappel libre/Rappel indicé à 16 items*: RL/RI-16 (Van der Linden et al., 2004). This verbal memory test is based on semantic cuing, that allows control of memory encoding and facilitates its retrieval. Sixteen words are presented to the participants, each associated with a category cue. Participants are asked to recall the words on three successive trials, and then to recognize the 16 items among 32 distractors before recalling them in a 30-min delayed trial. Each trial includes a free recall (FR) and a cued recall (CR), where the category cue is provided for the items not spontaneously recalled. The total recall score (TR) is the sum of the FR and the CR.

The Delayed Matching to Sample test-48 items (DMS-48 (Barbeau et al., 2004a) is a visual forced-choice recognition test. After an implicit encoding phase where 48 colored items are presented, an immediate (Set 1) and a one-hour delayed (Set 2) recognition trial are proposed asking participants to choose between the target and a distractor. Two different sets of distractors are used.

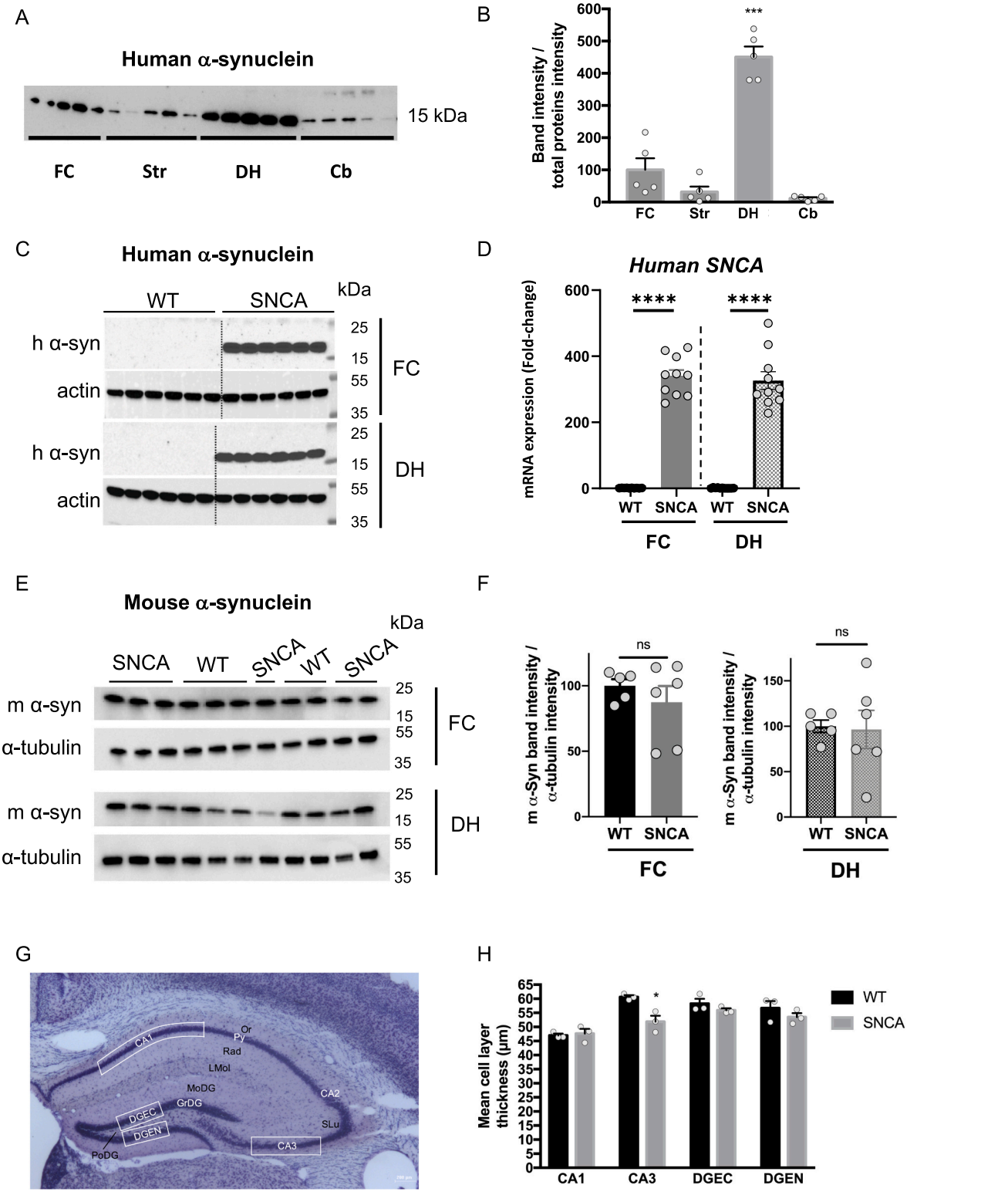

(caption on next page)

Fig. 1. Molecular and cellular characteristics of the Thy1-hSNCA mouse model. (A) Western blot analysis of human α-syn expression in various brain structures of the SNCA model and its Quantification. (B) Band intensity was corrected relative to that of total proteins from the same blot (see supplemental material, raw blot image). Levels in the FC were arbitrarily set at 100. Data are shown as mean ± SEM (n = 5/structure; *** p < 0,001 compared to all other structures, Tukey's multiple comparisons test). *FC, frontal cortex; Str, striatum; DH, dorsal hippocampus; Cb, cerebellum.* (C) Western blots performed with an antibody recognizing exclusively the human α-syn protein, thus confirming its expression in the FC and DH of SNCA mice and not in their WT littermates at 6 months of age. (D) RT-qPCR results showing expression levels of human SNCA gene, present only in SNCA mice in both FC and DH. (E) Western blots performed with an antibody recognizing exclusively the murine α-syn protein (m α-syn) in 12 months of age SNCA (n = 6) and WT (n = 5) brain lysates as noted. (F) Bar graphs showing quantifications of α-synuclein normalized to α-tubulin levels (±SEM). Endogeneous synuclein expression levels are not altered in the FC and DH of SNCA vs WT mice. WT were arbitrarily set at 100. Data were analyzed using unpaired t-test in SNCA (n = 6) vs WT (n = 5), *ns, non significant.* (G) Hippocampal coronal section stained by cresyl violet with labeled CA1, CA3 and DG regions (AP = bregma −1,94 mm). (H) Mean cell layer thickness of CA1, CA3 and DG limbs in WT and SNCA littermates at 14-month-old. Data are shown as mean of three different antero posterior levels per animal + SEM (n = 3/group; $ p < 0,05 compared to WT, t-test). *DGEC, ectal limb of DG; DGEN, endal limb of DG; Or, oriens layer; Py, pyramidal cell layer; Rad, radiatum layer; LMol, lacunosum molecular layer; GrDG, granule cell layer of the dentate gyrus; MoDG, molecular layer of the dentate gyrus; PoDG, polymorph layer of the dentate gyrus.* (For interpretation of the references to colour in this figure legend, the reader is referred to the web version of this article.)

The Frontal Assessment Battery (FAB; (Dubois et al., 2000) briefly assesses six cognitive functions sustained by the frontal lobes: conceptualization, mental flexibility, motor programming, sensitivity to interference, inhibitory control, and environmental autonomy. Three points are awarded for every perfect response (maximum score: 18).

2.18. Statistical analyses

Data are expressed as mean ± SEM. Statistical analyses were performed using Prism, version 7 and 8 (GraphPad software). A p-value ≤0,05 was considered as significant. Western blot and RT-qPCR data were analyzed with parametric Student t-test, or with one-way analysis of variance (ANOVA) when comparing more than two groups. Moreover, RT-qPCR samples were tested for outliers using the ROUT method with the Q value of 1 %, and the outlier, if detected, was excluded from the analysis. For behavioral data, we used Student t-test to analyze experiments with two unpaired groups, or two-way ANOVA with repeated measures for the MWM test. To compare a mean to a standard value, we used one-sample t-test. Normal distribution was tested using Shapiro-Wilk normality test, and if normality and/or homogeneity of variance were not respected, non-parametric tests were used instead of parametric ones: Mann-Whitney instead of Student t-test; Wilcoxon pair signed-rank test instead of one-sample t-test to compare mean (or median if non-parametric) to a hypothetical value.

In RT-qPCR experiments, ROUT outlier analysis (Q = 1 %) was performed on the sample groups resulting in exclusion of the detected outliers.

3. Results

Thy1-hSNCA mice used in this study were males of 12–14 months of age unless otherwise indicated in the text. Male mice were chosen to mimic the incidence of DLB that has been shown to be higher among men than women (Savica et al., 2013; Perez et al., 2010) and also to avoid large cohorts necessary to assess the sex effect. The age of the mice was chosen as to ideally model early/prodromal stages of the disease and avoid age-related cognitive impairment versus disease-related ones (Yanai and Endo, 2021). Mouse model overexpressing the wild-type form of synuclein are not expected to elicit strong symptoms from an early age (compared to the ones expressing mutant ones) (Crabtree and Zhang, 2012; Hatami and Chesselet, 2015), so younger mice were not tested in this study.

3.1. The Thy1-hSNCA mouse model shows high levels of the pathological form of α-synuclein in the frontal cortex and dorsal hippocampus

Protein expression of the human synuclein was assessed throughout various brain structures in SNCA mice: frontal cortex (FC), striatum (Str), dorsal Hippocampus (DH) and cerebellum (Cb) (Fig. 1A, B). Levels in the DH were significantly higher than in other structures (4.5-fold compared to FC, 14.1-fold, compared to striatum and 38.6-compared to cerebellum (p < 0.001) (Fig. 1B). Expression of human synuclein protein was also higher in the frontal cortex than in the striatum and cerebellum but not significantly (p = 0.274 and p = 0.109, respectively), although transgene expression was described as more abundant in the frontal cortex (strain #016936). When assessed in both WT and SNCA mice, the human α-syn expression was exclusively detected in the FC and DH of the SNCA model, both at the protein (Fig. 1C) and mRNA (Fig. 1D) levels, therefore confirming the genotypic validity of the model. Importantly, synuclein protein levels (Fig. 1E, F), nor mRNA levels (Fig. S1A) of endogenous murine α-syn in these structures did not differ between SNCA and WT subjects showing that transgene insertion did not impede the expression of the endogenous α-syn and that any pathology present in the model will arise solely from the hSNCA over-expression. Lastly, as the SNCA transgene is inserted into the *Slc4a7* gene locus, we checked its regulation by RT-qPCR and found a significant two-fold downregulation of gene expression, which was equally detected in both FC and HD (Fig. S1B).

We performed morphometric measurements of the hippocampal CA1, CA3 and DG cell layer thickness (Fig. 1G) and observed a decrease in CA3 thickness in the SNCA compared to WT mice (p = 0.017, Fig. 1H). CA1 and DG regions from SNCA mice did not present any difference in cell layer thickness relative to WT mice (Fig. 1H).

We then assessed the presence of pathological forms α-syn with an antibody targeting the serine 129 phosphorylated form (pSyn129) of synuclein from both murine and human origin. Data were compared to the levels of total (murine and human) α-syn level. As expected, we found increased levels of total α-syn levels in the FC, DH and Str of the SNCA mice (by 2-fold, p < 0.001; 1.7-fold, p < 0.001; 2-fold, p < 0.01 respectively) (Fig. 2A, B). The expression of pathological pSyn129 was also significantly higher in SNCA compared to WT in all three structures (7.7-fold in FC, p < 0.001; 6.8-fold in DH, p < 0.001; 2.5-fold in Str, p < 0.01) (Fig. 2C), but the ratio of pSyn129 to total α-syn was only significantly increased in the FC and DH of SNCA mice compared to control (by 4.1-fold, p < 0.001; by 3.6-fold, p < 0.001) (Fig. 2D).

The pSyn129 increase in the SNCA model was corroborated by immunohistochemical analysis, with detected presence of varying types of pSyn129-positive inclusions (Fig. 2E): relatively homogeneous somatic type markings (arrows); others that are not homogeneous and appear rather fibrillar but still somatic (chevrons); and finally, neurite-type markings (arrowheads). These inclusions were found in the FC; including the infralimbic (IL), prelimbic (PrL) and anterior cingulate (Cg) cortices; secondary motor (M2) and agranular insular (AI) cortices; as well as in the primary somatosensory (S1) and primary motor (M1) cortices of SNCA, but not WT mice (Fig. 2F). They were also present in the DH, especially in its CA3 and CA1 pyramidal layers, while not in the granular layer of the DG (Fig. 2G). Overall, diffuse pSyn129 marking could be observed throughout the cortex, especially in insular (IC), perirhinal (PRh) and lateral entorhinal (LEnt) regions (Fig. S1C), as well as in the basolateral amygdaloid nucleus (BLA) (Figs. S1D, E). However, dopaminergic structures such as Str and the *substantia nigra pars compacta* (SNc) did not show any labeling against pSyn129 (Fig. S1D). It can

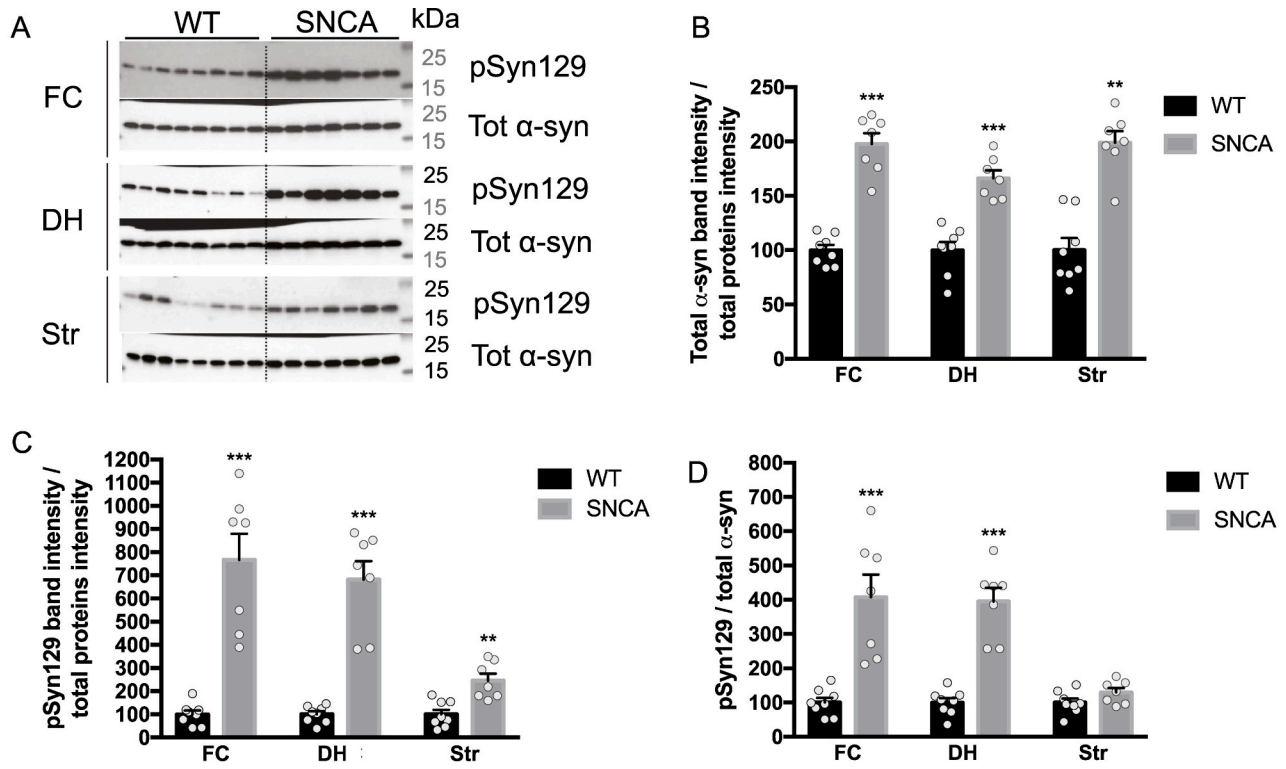

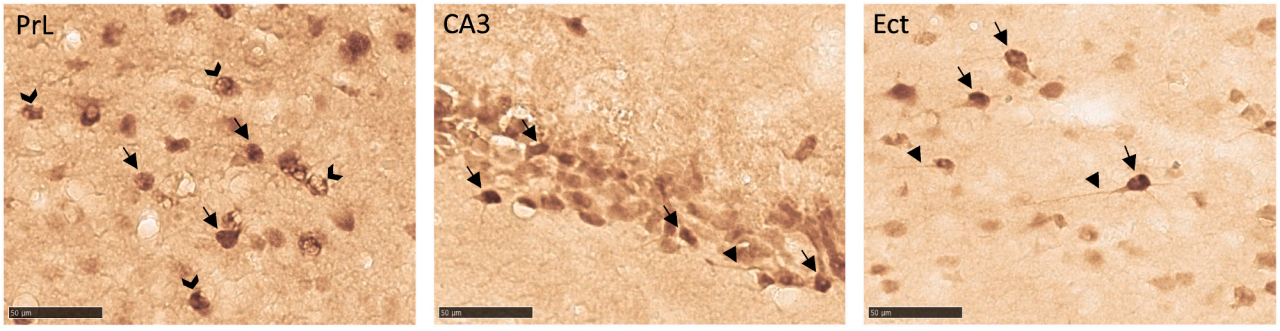

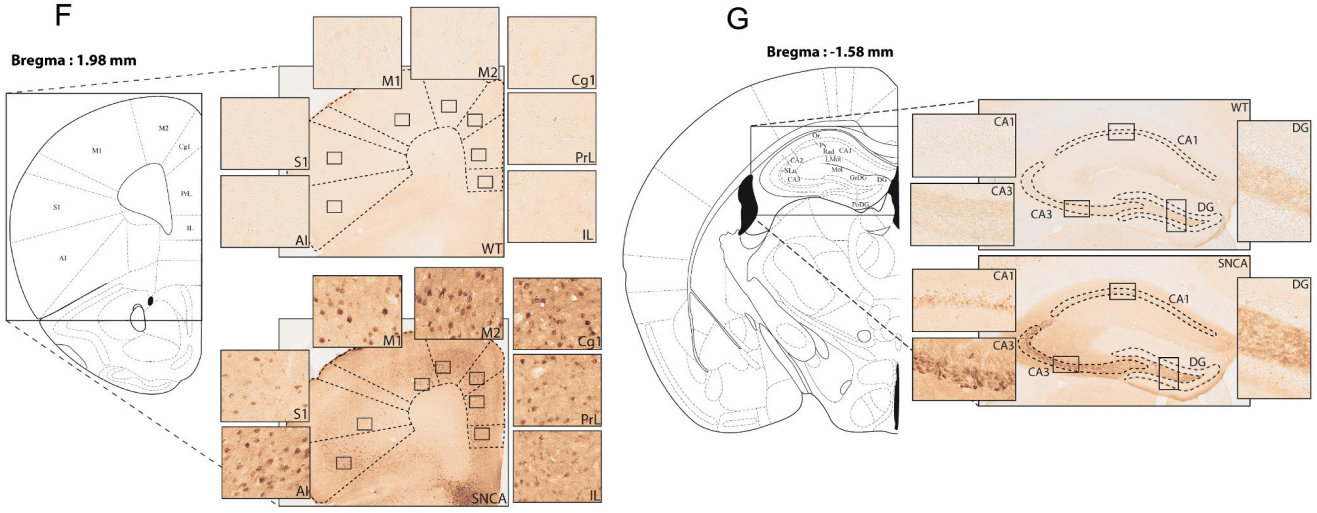

(caption on next page)

Fig. 2. Pathological phospho-Syn129 levels are highest in the FC and DH of SNCA mice. (A) Representative western blots comparing phosphorylated (18 kDa) and total α-syn (15 kDa) protein levels in the FC, DH and Str of WT and SNCA mice. (B—D) Corresponding quantification of the western blots. Levels found in WT mice are arbitrarily set at 100. Band intensity was corrected relative to that of total proteins from the same blot (see supplemental material, raw blot image). Data are shown as mean ± SEM (WT, $n = 8$; SNCA, $n = 7$; ** p < 0,01, *** p < 0,001 compared to WT, two-tailed *t*-test). (B) Total α-syn. (C) pSyn129. (D) pSyn129 / total α-syn ratio. *FC, frontal cortex; DH, dorsal hippocampus; Str, striatum.* (E) pS129 immunohistochemistry performed on frontal sections of SNCA mice showing homogeneous somatic (arrows), fibrillar-like (chevrons) and neurite-like markers (arrowheads). (F,G) Immunohistochemistry showing pSyn129 in the FC, S1 and M1 (F) or DH (G) of the SNCA mice (bottom panel) vs WT littermates (upper panel). *AI, agranular insular cortex; Cg1, cingulate cortex area 1; DG, dentate gyrus; IL, infralimbic cortex; M1, primary motor cortex; M2, secondary motor cortex; PrL, prelimbic cortex; S1, primary somatosensory cortex; Ect, ectorhinal cortex.*

be noticed that the fibrillar (chevron) somatic labeling was exclusive for cortical structures, not appearing in limbic ones (DH and BLA), while neurite-type marking was the least represented form of pSyn129-positive inclusions in both (DH and Ect).

As pSyn129-positive inclusions were detected in the hippocampus, we verified by western blot whether the SNCA model would present aggregates at this age (12-month-old male mice). The proteins were separated into Triton-soluble (SF) and insoluble (IF) fractions for comparison (Zhou et al., 2008). We observed that both synuclein and phospho S129 synuclein levels were significantly higher in SNCA mice, but only in the soluble fraction (Fig. S2A). Further, accumulation of oligomers was not detected in this fraction in the SNCA mice. Indeed, even though some higher molecular weight bands appeared, they were equally detectable in the WT and SNCA mice (Suppl, S4). These upper bands were also detected at different molecular weights with the α-syn and the pSyn129 antibodies (45 and 100 KDa for α-syn and 35 and 130 KDa for pSyn129). Importantly, they did not correspond to the usual ruler pattern of oligomers as observed between 50 and 130 KDa in brain structures from another synuclein over-expressing mouse model at later stage of the disease (see Fig. 3 from Zhou et al., 2008). They were thus considered as nonspecific bands (Suppl, S4). This suggests that at this stage (12 months of age), synuclein is hyperphosphorylated but remains soluble and nonaggregated. The absence of aggregates was further confirmed by thioflavinS staining, in both the hippocampus and the frontal cortex, as no labeling was observed compared to that obtained in tissues from THY-Tau22 mice, modeling tau aggregation, used as positive control of protein aggregate presence (Fig. S2C).

3.2. SNCA mice show FC-related cognitive deficits and spared HD-related ones

We tested spatial reference memory in the SNCA model at 12 months of age using the Morris water maze test (MWM) (Fig. 3A, B). This type of memory relies primarily on the hippocampus and its interplay with other structures such as the prefrontal cortex - depending of the phase of memory: acquisition, encoding or long-term (recent and remote) retrieval (Maviel et al., 2004; Lopez et al., 2012). First, we observed that during the acquisition phase, the distance travelled to reach the platform decreased ($F(4.132) = 32.05$; $p < 0.001$) in both groups ($F(1.33) = 1.97$; $p = 0.169$) (Fig. 3C), indicative of successful learning. Recent (24 h) and remote (21d) memories were tested. WT and SNCA mice spend more time than chance (15 s) in the SE target quadrant ($p < 0.001$) (Fig. 3D) at both retention times, showing proper hippocampal function. However, at 21d post-acquisition the SNCA mice spend significantly less time in the target quadrant ($p < 0.05$) (Fig. 3D) and in the platform/annulus zone ($p < 0.05$) when compared to the WT ones (Fig. 3E), suggesting possible deficits in hippocampo-cortical interactions. We also tested spatial memory of the transgenic model using an object location test with 3 h recall time (Fig. 3F). The result was expressed as percentage of time spent exploring the moved object from the total exploration time for all objects present. Both WT and SNCA mice explored the displaced object significantly more compared to random ($p < 0.001$) and there was no difference in exploration time between the genotypes ($p = 0.642$) (Fig. 3G), emphasizing again proper hippocampal function.

We then tested the Novel Object Recognition (NOR) task at a 3-h delay (Fig. 4A). The WT mice explored the new object to a greater extent compared to random ($p < 0.001$) (Fig. 4B). However, although the percentage of time the SNCA mice that explored the new object did not differ from that of the WT ($p = 0.512$), it was not significantly different from chance ($p = 0.077$) (Fig. 4B), suggesting a mild deficit in this task. Lastly, we tested the object-in-place (OiP) task (Fig. 4C). WT ($p = 0.001$) but not SNCA ($p = 0.944$) mice showed significantly higher exploration rate of the changed object compared to chance (Fig. 4D). Compellingly, the percentage of time spent exploring the object that had been changed differed significantly between genotypes ($p = 0.023$; $p < 0.05$), showing OiP deficit in the SNCA model. These two last object memory tests point to possible dysfunctions related to frontal and perirhinal structures in the SNCA model (see discussion).

3.3. The SNCA model does not show motor deficits

We then checked motor functions with actigraphy and the bar test. The locomotor activity of the SNCA mice tested over 48 h showed no alteration during the night/day cycle ($F(1.17) = 1.803$; $p = 0.1971$; Fig. 5A). We verified the status of dopaminergic neurons in the 12-month-old SNCA mice. We did not detect any significant change in dopaminergic neurons in the substantia nigra (Fig. 5B) or dopamine nerve terminals in the striatum (Fig. 5C), suggesting that midbrain dopamine neurons are not affected in SNCA mice, in line with the absence of detectable pS129syn in these regions (Fig.S1D). As motor symptoms, unlike cognitive, are often not as prevalent until more advanced stages of DLB, we opted for an older cohort of 18 months of age to test motor functions, considering SNCA mice presented only mild cognitive deficits at 12–14 months of age. Motor coordination was tested using the beam crossing test. We found that the average time taken by the WT and SNCA mice to cross the bar did not differ (Fig. 5D), as did not the number of errors (Fig. 5E) and errors per step (Fig. S3A). Thus, global motor coordination of the SNCA model does not seem to be affected, as old as 18 months. We then used the nest building test at different delays to detect fine motor deficits. Compared to the WT, SNCA mice did not display any deficits in nest construction and achieved a good score quality, regardless of the time delay (Fig. S3B, C). Lastly, we tested another type of memory with novel taste learning, suggested to rely on insula and frontal cortex interactions (Kayyal et al., 2021). Prior to this, the buried food-seeking test was performed to assess any olfactory deficits present in the model and no change in the average time taken to detect food was found between genotypes, with average of 53.29 s and 57.88 s for WT and SNCA groups, respectively ($p = 0.652$) (Fig. S3D). Then, the “novel taste learning” test demonstrated no genotype-related differences (Fig. S3E), where the SNCA mice assimilated to the new taste as adequate as the WT did, showing the same degree of neophobia towards new food.

3.4. Neuronal plasticity marker proteins are down-regulated only in the FC of SNCA mice

The next step was to determine molecular changes occurring in the SNCA mouse model. We then assessed several neuronal plasticity markers by western blot analyses in three different regions of the brain: the frontal cortex (Fig. 6A-D), the dorsal hippocampus (Fig. 6E-H) and the Striatum (Fig. S4A—D). We detected a significant down-regulation of the protein level of SYP I, RAB10 and PSD95 (respectively, by 50 %, $p < 0.001$; 31 %, $p < 0.01$; and 36 %, $p < 0.05$) in the FC of SNCA mice (Fig. 6A, B). However, this decrease was observed neither in their DH

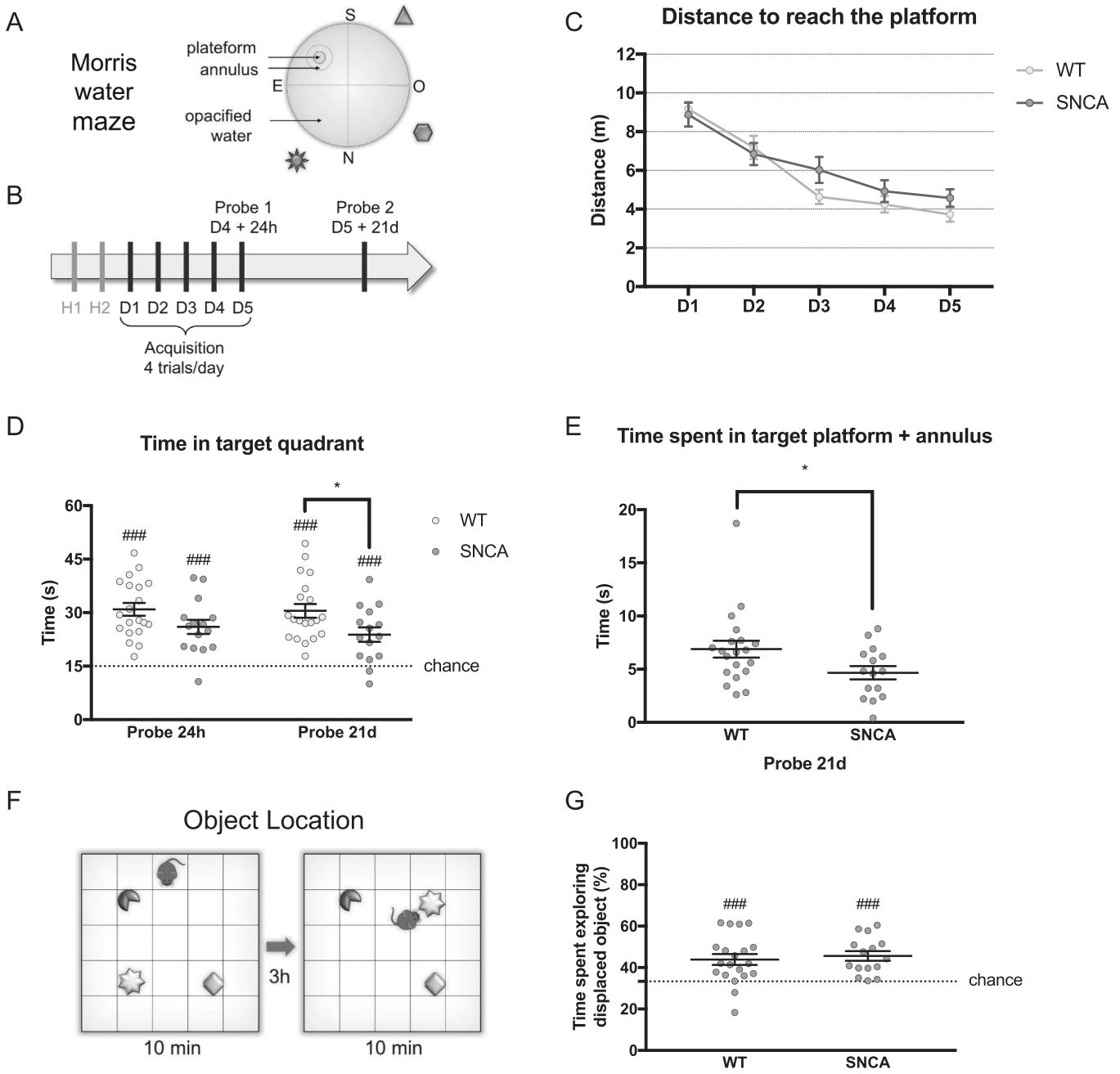

Fig. 3. SNCA mice display no deficits for hippocampal-dependent recent spatial memory tasks, but are less performant in remote memory. (A) Sketch of the Morris water maze (MWM) device and (B) of the protocol used. The platform is placed in the SE quadrant, submerged in opacified water and surrounded by several distal spatial cues. After 2 days of habituation, mice undergo 4–5 days of acquisition (4 trial/day) and are subjected to 2 probe tests, one for recent long-term memory (after 24 h) and one for remote memory (after 21 days). (C) Distance travelled to reach the platform decreases during acquisition for both SNCA and WT groups. (D) Both WT and SNCA mice spent more time in the target quadrant compared to chance (15 s) 24 h and 21 days post-acquisition. However, SNCA mice spend significantly less time in the target quadrant than the WT mice at the 21d probe test. (E) SNCA mice spent significantly less time in the platform + annulus zone 21-days post-acquisition, compared to the WT mice. WT, $n = 20$; SNCA, $n = 15$. (F) Object location protocol. Mice are tested during 10 min, 3 h after the 10 min-acquisition period. (G) Time spent exploring the displaced object in the object location task. Both WT and SNCA mice show notably higher exploration rate of the displaced object compared to chance (33 %). There is no significant difference in time spent exploring the new object between groups. WT, n = 20; SNCA, n = 15.
Data are shown as mean ± SEM; ### $p < 0{,}001$ compared to chance, one sample *t*-test; * $p < 0{,}05$ compared to WT, two-tailed t-test.

(Fig. 6E, F) nor in their Str (Fig. S4A, B). The postsynaptic markers NRGN did not present altered expression in all the three structures (Fig. 6A, B, E, F; S4A, B). Furthermore, NEUN and GFAP protein levels were not altered between SNCA and control in the FC (Fig. 6C, D), DH (Fig. 6G, H) or Str (Fig. S3C, D). Additionally, a series of RT-qPCR analyses targeting these plasticity markers were performed on the FC and DH (Fig. S5). Unlike protein levels, the mRNA levels of plasticity markers (*Syp, Dlg4, Rab10)* remained unchanged in the FC, as well as in the DH of SNCA mice (Fig. S5A—C), with *Dlg4* even showing an upregulation tendency in the FC ($p = 0.1$; Fig. S5B). There was no detected change in expression of *Gfap* in neither FC nor DH (Fig. S5D).

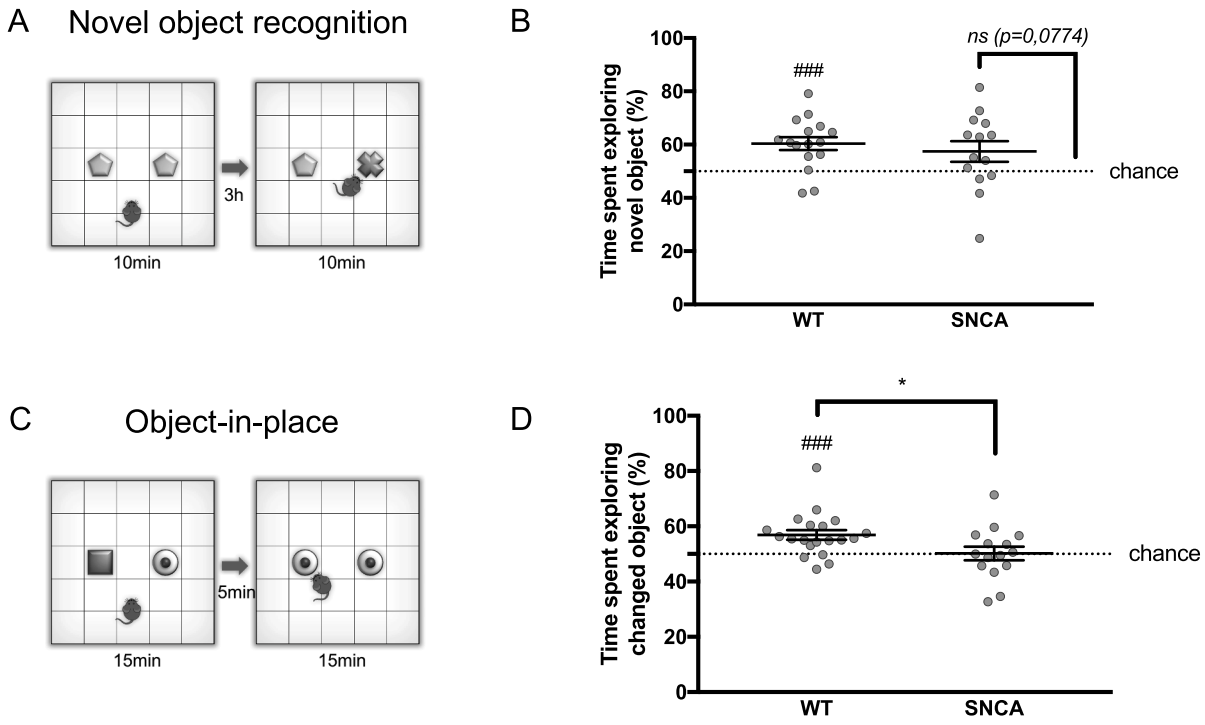

Fig. 4. Object recognition memory is partially affected in the SNCA model. (A) Novel object recognition protocol. Mice are tested during 10 min, 3 h after the 10 min-acquisition period. WT but not SNCA mice show significantly higher exploration rate of the novel object compared to chance (50 %). There is no significant difference in time spent exploring the new object between groups. WT, $n = 16$; SNCA, $n = 14$ (B) Object-in-place protocol. Mice are tested during 15 min, 5 min after the 15 min-acquisition period. WT mice show a significantly exploration rate of the changed object compared to chance (50 %), while SNCA mice remain at chance levels. There is a significant difference between WT and SNCA mice in time spent exploring the displaced object. WT, n = 20; SNCA, n = 15.
Data are shown as mean ± SEM; * p < 0,05, two-tailed t-test or Mann-Whitney; # p < 0,05, ### p < 0,001 compared to chance, one sample t-test.

3.5. Transcriptional upregulation of inflammatory markers in the FC of SNCA mice

As neurodegenerative diseases are often accompanied by neuro-inflammation, we checked a series of inflammatory markers by RT-qPCR (Fig. 7, S6). We found significant transcriptional upregulation of inflammatory markers in the FC ($p \leq 0.05$), with again, no change in the DH (Fig. 7) of the 14-month-old SNCA mice. Among the upregulated genes in the FC were complement component *C1qa* (Fig. 7A) and pro-inflammatory cytokines *Il1b,* and *Tnf* (Fig. 7B, C). *Ifngr2* (a proinflammatory cytokine related to interferon gamma), which showed a trend towards higher levels in the FC of SNCA mice ($p = 0.15$) compared to WT. Compellingly, the transcription of *Cd68*, a marker of macrophage/microglial endocytosis, was upregulated, while that of *Aif1* (the microglial marker Iba1) was down-regulated in the FC of SNCA mice. None of these markers were changed in the DH (Fig. 7). Not all evaluated inflammatory markers showed upregulation, and such were *Tgfb1, Ccl4, C3, Il6* and *Itgax* (Fig. S6A-E). Even though not reaching significance, we noted that *Ccl4* and *Itgax* displayed noticeably elevated expression in SNCA FC compared to WT FC (Fig. S6B, p = 0,14 and Fig. S6E, p = 0,15 respectively). Inflammatory markers were also checked at the level of the protein, by immunohistochemistry using Iba1 and GFAP in the mPFC (Fig. S7) and DH (Fig. S8). Intensity of immunofluorescence and density of cells within regions of interest were counted in mPFC and DH and no significant difference was observed.

In sum, our studies performed in the SNCA mouse model at 12–14 months of age documented a clear impairment observed of their FC, characterized by associated cognitive deficits, loss of plasticity markers and increase of inflammatory markers, while the dorsal hippocampus and other structures as the striatum and substantia nigra seemed more preserved.

3.6. Prodromal-DLB patients display FC-related cognitive deficits

In an attempt to ascertain whether the SNCA model could be a good fit for DLB-related studies in animal, we drew a comparison between the pathophysiological deficits observed throughout our study with those detected in a cohort of prodromal DLB patients (pro-DLB). This comparison was possible owing to the results obtained from the AlphaLewyMA study that includes 34 healthy elderly control subjects (HC) and 55 pro-DLB patients (https://clinicaltrials.gov/ct2/show/NCT01876459).

The results of the 16-item Free and Cued Recall test (RL/RI-16, see material and methods) showed a deficit in free recall (FR) (24.89 vs 30; $p < 0.001$) as well as in total recall (TR) (44.33 vs 46.06; $p = 0.026$, $p < 0.05$) in the pro-DLB subjects compared to HC. For both groups the TR score was higher than that of the FR ($p < 0.001$), indicating that indexing ameliorated the score regardless of pathology presence (Fig. 8A). Overall, both HC and pro-DLB subjects improved their FR and TR scores significantly over the span of three recalls (Fig. S9A). Nonetheless, the score attributed to the pro-DLB cohort was still significantly lower than that of the HC at the time of the last recall (R3) (FR $p < 0.001$; TR $p = 0.005$, $p < 0.01$) (Fig. S9A). In addition, pro-DLB cohort obtained a notably lower score in the Frontal Assessment Battery (FAB) test compared to HC ($p < 0.001$) (Fig. 8B).

The results of the DMS48 test, a visual recognition memory test designed to detect memory changes early on in dementia progression (Rullier et al., 2014), showed a significant deficit of immediate and delayed recognition in pro-DLB cohort (respectively $p = 0.001$; and $p = 0.005$, $p < 0.01$), more pronounced for the former one. The mean score between delayed and immediate recognition did not differ in either HC (respectively 47.06 vs 46.96, $p = 0.857$) or pro-DLB cohort (respectively 44.67 vs 44.81, $p = 0.971$) (Fig. 8C). Ultimately, the pro-DLB subjects took longer than HC to complete the acquisition ($p = 0.009$, $p < 0.01$)

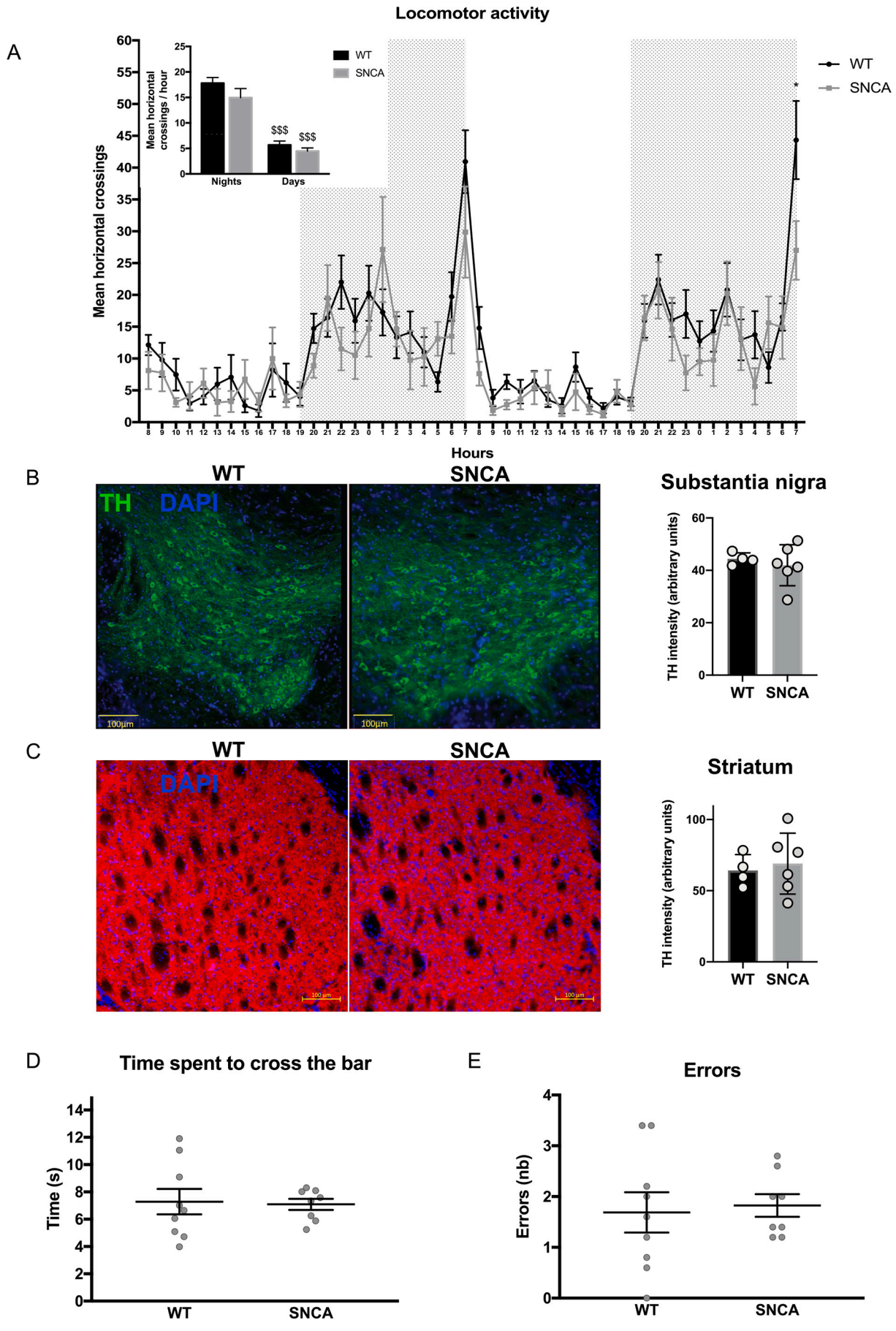

(caption on next page)

Fig. 5. SNCA mice do not show motor deficits nor TH deficiency. (A) Actigraphy performed at 14 months of age. Locomotor activity of WT and SNCA mice is represented by the number of horizontal crossings per hour during two nights and two days (repeated measures ANOVA: hours effect $F_{(47,887)} = 11,33$, $p < 0,001$, no genotype effect $F_{(1,21)} = 2408$, $p = 0,136$; Sidak multiple comparisons test: Night 2, 7 h $p = 0,011$, $p < 0,05$). Insert: mean horizontal crossings per hour during nights and days (repeated measures ANOVA: nights/days effect $F_{(1,21)} = 141,3$, $p < 0,001$; Sidak multiple comparisons test: nights vs days, WT and SNCA p ⟨0,001). Data are shown as mean ± SEM (WT, n = 15; SNCA, n = 8). $$$ $p < 0,001$ compared to nights. (B, C) Tyrosine Hydroxylase (TH) immunochemistry performed on 12-month-old WT and SNCA mice showing dopaminergic neurons in the substantia nigra (Fig. 5B) (green, upper panel) and their terminals in the striatum (Fig.5C) (red, lower panel). Nuclei are labeled with DAPI staining (blue). Representative images are shown. Bars: 100 μm. Bar graphs (±SEM) on the right represent quantification of fluorescence intensity (QPath) in WT ($n = 4$) and SNCA ($n = 6$) mice and show no statistical difference between genotypes, Unpaired *t*-test. (D, E) Bar test performed at 18 months of age. The time spent to cross the bar (Fig. 5D) and the mean number of errors (Fig. 5E) are similar between WT and SNCA mice (Student t-test: $p = 0,776$). Data are shown as mean ± SEM (WT, $n = 9$; SNCA, n = 8). (For interpretation of the references to colour in this figure legend, the reader is referred to the web version of this article.)

(Fig. S9B) and immediate recognition ($p = 0.0096$, $p < 0.01$) (Fig. S9C) phases of the test. This set of data is corroborating the notion of FC-associated impairment in the early stages of DLB. In all, comparison of these results with those obtained in the SNCA mouse model (Fig.8D) led us to suggest that the 12-month-old mThy1-hSNCA mouse model parallels numerous early markers of this pathology.

4. Discussion

To date, only a few animal models have been developed with the intention of mimicking DLB (Zhou et al., 2008; Lim et al., 2011) and this paucity of models is hampering DLB-research progression. In the current study, we engaged in a thorough phenotypic characterization of a novel model overexpressing the wild-type form of human α-syn (strain #016936). Since the prevalent overexpression of the transgene was detected in the FC and DH, and not Str, we had strong reasoning to believe this model to be more suitable for DLB-related research. Our study led with an extensive battery of behavioral approaches on the SNCA model, uncovered specific cognitive deficits associated with the FC rather than with the DH, while no motor dysfunctions and no dopaminergic alterations were detected. Further, while pathological pSer129 synuclein was up-regulated in both FC and DH, without detection of aggregated forms, synaptic neuronal markers were down-regulated at the protein levels, and gene expression of inflammatory markers was up-regulated specifically in the FC, emphasizing the susceptibility of this structure in this model. Lastly, behavioral tests led on a cohort of prodromal DLB patients versus age-matched controls showed that at this prodromal stage, deficits are more associated with the FC. Therefore, the SNCA model that was phenotyped in this study might be considered a new model of early stage DLB.

4.1. Cognitive dysfunctions in the SNCA mice compared to prodromal DLB patients

In the SNCA mouse model, we detected FC-dependent deficits in the MWM and OiP tests. More specifically, in the MWM task, 21 days after acquisition, SNCA mice spent significantly less time in the target quadrant than their WT counterparts, indicating the presence of long-term remote memory deficits emanating either from FC dysfunction or impaired hippocampal-frontal cortex functional interconnectivity required for memory retrieval and/or systemic consolidation (Maviel et al., 2004). Since hippocampal function appears to be preserved during spatial encoding in the MWM and object location tests, and since there is no deficit in spatial object memory recovery after a short delay (3 h), we can argue that the deficit might implicate dysfunctions in the FC. In the OiP task, which is an associative memory test, there is a clear deficit in SNCA mice due to their lack of target object exploration, not differing from random, and their significantly lower comprehensive exploration of the changed object compared to WT mice. OiP deficiency suggests an impairment of lateral entorhinal cortex (Lent) and/or perirhinal cortex (PRh) but may also be due to the impairment of the median prefrontal cortex (mPFC) (Barker et al., 2007; Chao et al., 2016). During the NOR task, SNCA mice did not explore the new object differently from random, although their overall performance did not differ from that of the WT littermates. The NOR task with a 3-h delay more specifically involves the PRh, as its role is crucial in discrimination between a novel and a familiar object (Barker et al., 2007; Brown and Aggleton, 2001). It could therefore be deduced that there is also a probable impairment of the PRh in SNCA mice, as PRh thickness was reported to be reduced in DLB, but not AD patients (Delli Pizzi et al., 2016). Conversely, we did not observe any major deficit of the olfactory capacity of SNCA mice, that is commonly observed in both early PD (Doty, 2012; Driver-Dunckley et al., 2014; Fullard et al., 2017) and DLB patients (Chiba et al., 2012; Thomas et al., 2022). Furthermore, in the novel taste learning, both WT and SNCA mice pre-exposed to the new food showed an absence of neophobia towards it, accounting for successful acquisition of the novel taste. This test is underpinned by the insular cortex (IC) (Swank and Sweatt, 2001; Moraga-Amaro et al., 2014; Yiannakas and Rosenblum, 2017), which is believed to be among the first atrophying regions in DLB patients (Blanc et al., 2015; Blanc et al., 2016; Roquet et al., 2017), signifying no major functional impairments of the IC in SNCA mice at this age. Importantly, the SNCA model does not show major motor deficits even at 18 months of age, supporting the idea that the SNCA model rather mimics DLB than PD, given the significantly lower prevalence of motor symptoms in DLB patients compared with those seen in PD (Jellinger, 2019). It is noteworthy that the a-synuclein and pSyn129 levels detected seemed to be only of the soluble form, with no oligomers formations at that stage of the disease, maybe a reason why severe deficits such as motor ones are not detected. This may be attributed to the fact that the SNCA model of this study overexpresses a wild-type form of SNCA and not a mutated one, as compared for example to the study of Zhou et al. (2008), in which of the synuclein Y39C mutation is also overexpressed under Thy1 promoter, and produced progressive oligomer formation, aggregates and motor deficits. It is documented that overexpression of mutated SNCA models often gives stronger motor deficits (Crabtree and Zhang, 2012; Hatami and Chesselet, 2015) which is not the case in our model. Oligomers may appear at later stages because duplication/triplication can induce dementia related to DLB and PD (Singleton et al., 2003; Meeus et al., 2012).

Interestingly, this pattern of FC functional deficiency with preserved DH one was observed in prodromal DLB patients from the AlphaLewy study, who recorded lower scoring in the RL/RI-16 and FAB tests compared to HC, indicating that the SNCA model is successful in mimicking functional deficits present in early stage DLB patients. Indeed, pro-DLB patients have a significant deficit of free recall (RL) and total recall (RT) in the RL/RI-16 task, specialized for detecting very mild dementia (Grober et al., 2010) classically related to frontal deficiency (Philippi et al., 2016). Cued recall, however, increased the score of pro-DLB patients, like that of HCs, further suggesting that the deficit is not of hippocampal origin. As a matter of fact, in AD patients affected by hippocampal impairment, cued recall does not result in improvement of the patient's score (Van der Linden et al., 2004). Accordingly, the FAB, which specifically tests for frontal lobe emanating deficits (Dubois et al., 2000), has also highlighted presence of such alterations in the pro-DLB cohort. On the other hand, the pro-DLB group displayed significantly greater shortfall for immediate, compared to delayed recognition in the DMS48 test, with this pattern of cognitive decline being linked to deficits of the parahippocampal gyrus, including LEnt and PRh cortices (Barbeau

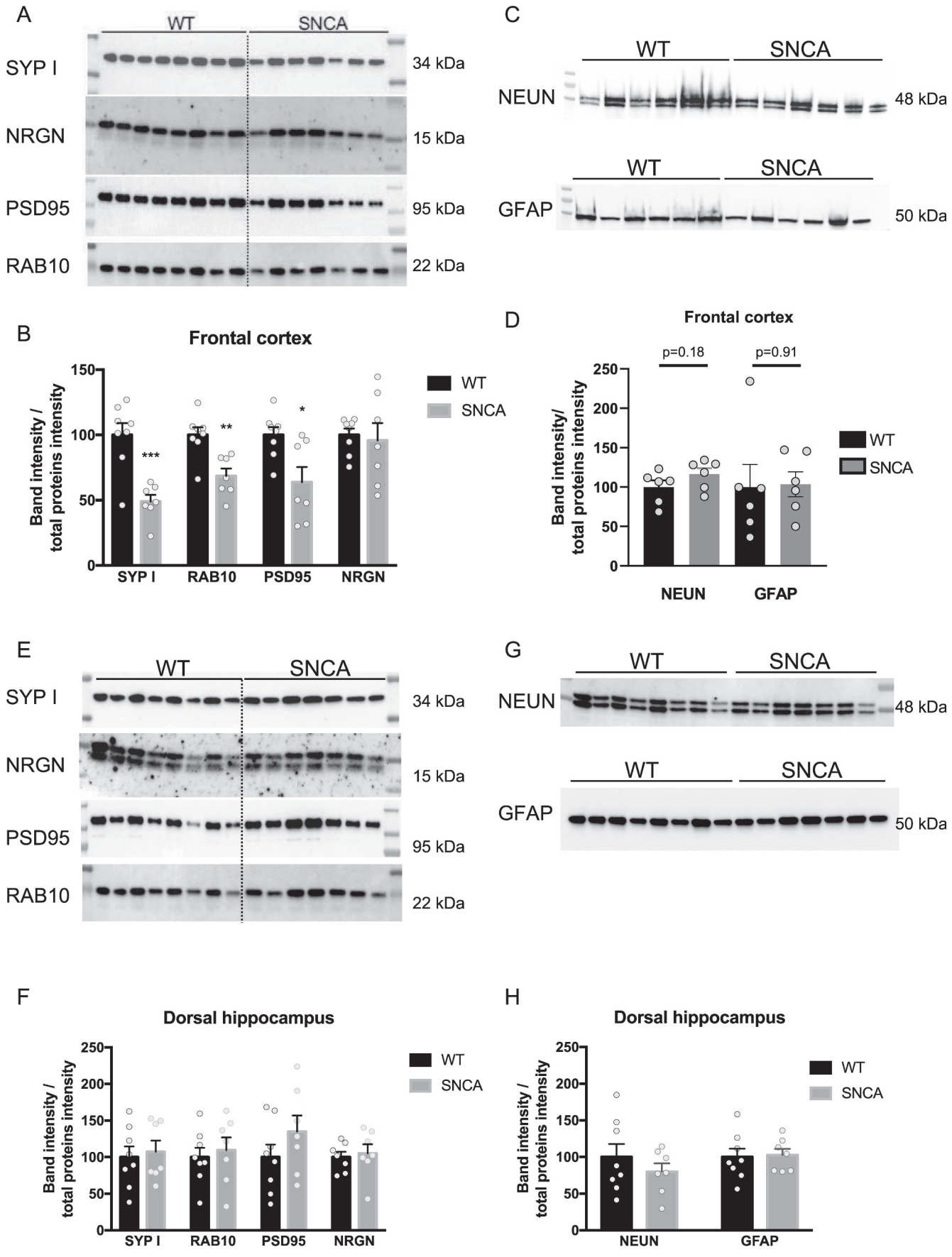

(caption on next page)

Fig. 6. Protein levels of plasticity makers are reduced in the FC of SNCA mice, but not in the DH. Representative western blots comparing protein levels of neural plasticity markers between SNCA (n = 7) and WT (n = 8) littermates and its quantification in the frontal cortex (A,B) and the dorsal hippocampus (E,F). Representative western blots comparing NEUN and GFAP protein levels between SNCA (n = 7) and WT (n = 8) littermates and its quantification in the frontal cortex (C,D) and the dorsal hippocampus (G,H). Band intensity was corrected relative to that of total proteins from the same blot (see supplemental material for raw blot images). Data are shown as mean ± SEM; * p < 0,05, ** p < 0,01, *** p < 0,001 compared to WT controls, two-tailed t-test or Mann-Whitney). *SYP, synaptophysin I; RAB10, Ras-Related GTP-Binding Protein; PSD95, Postsynaptic density protein 95; NRGN, neurogranin; NEUN, neuronal nuclear protein; GFAP, glial fibrillary acidic protein.*

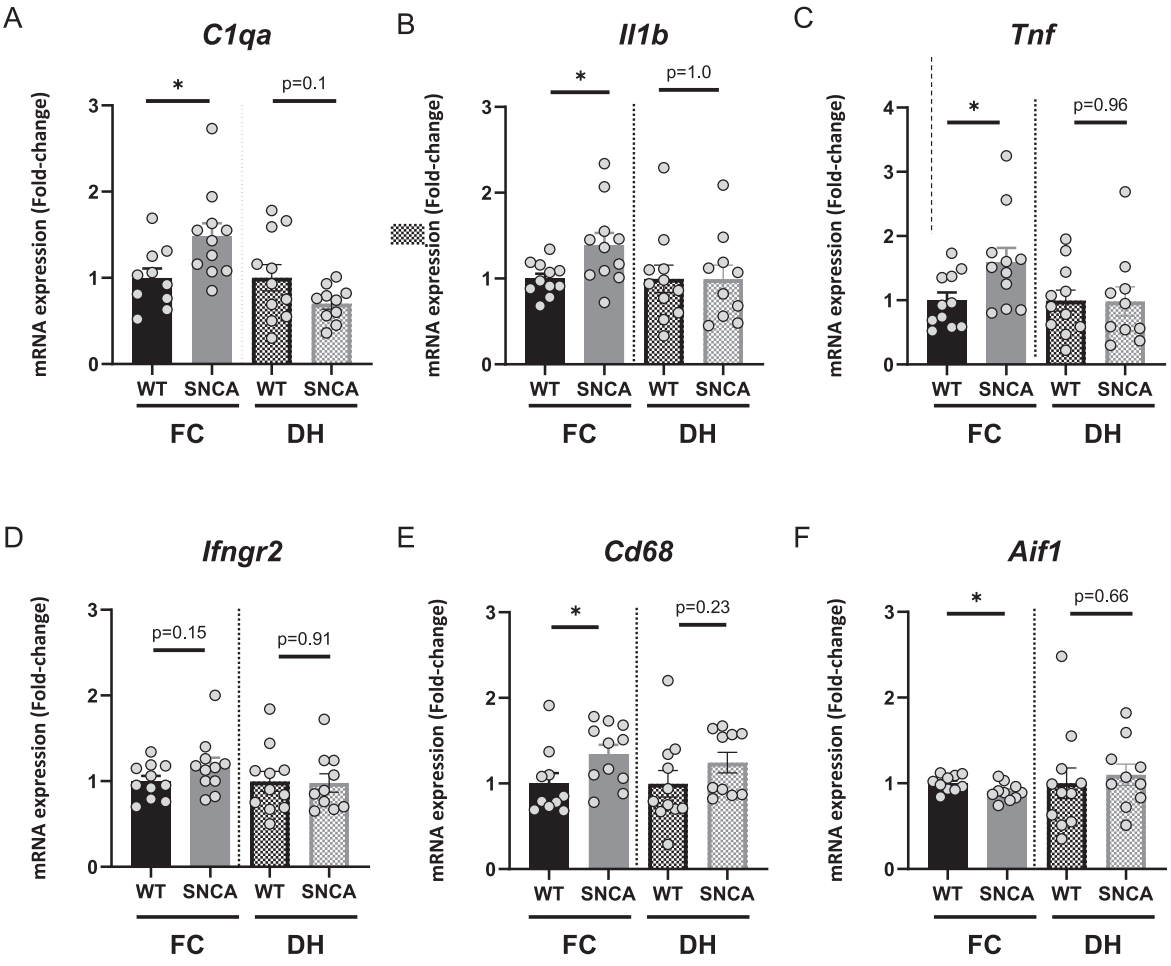

Fig. 7. Transcript levels of inflammatory genes that are dysregulated in the FC but not DH of SNCA mice. (A-F) RT-qPCR results showing mRNA expression levels of inflammatory markers in the FC and DH of SNCA and WT mice, (A) *C1qa* (B) *Il1β* (C) *Tnf* (D) *Ifgnr* (E) *Cd6.* (F) *Aif1.* Data are shown as mean ± SEM (WT, $n \leq 11$; SNCA; $n = 11$). * p < 0,05, ** p < 0,01, *** p < 0,001 compared to WT, unpaired t-test. ROUT outlier analysis (Q = 1 %) was performed on the sample groups resulting in exclusion of the detected outliers. *C1qa, Complement C1q A Chain; Il1β, Interleukin 1 beta; Tnf, Tumor necrosis factor; Ifngr2, Interferon gamma receptor 2; Cd68, Cluster of Differentiation 68; Aif1, Allograft inflammatory factor 1.*

et al., 2004b; Philippi et al., 2016). Along this line, the previously mentioned impairments of the SNCA model in the OiP and NOR tasks, relying on the proper functionality of the aforementioned structures, is consistent with deficits detected in pro-DLB patients. Our results obtained in the SNCA mouse model is also in agreement with the recent study by Oppedal et al. (2019) which determined by MRI, a hippocampal-sparing cortical atrophy pattern signature in a study including 333 DLB patients.

4.2. Molecular, cellular and anatomopathological insights into the SNCA mouse model

WB and IHC analyses showed a strong pSyn129 increase in the FC and DH, that was absent from the Str, which is consistent with the absence of motor symptoms in the model. It is also interesting to note that the IHC labeling was not observed in SN which is particularly affected in PD. These data are coherent with the fact that we did not detect alteration of dopamine neurons in the SN, nor of their striatal terminals, again arguing in favor of mimicking a DLB model rather than a PD model. Interestingly, the BLA structure was also greatly affected by the diffuse pSyn129 labelling, consistent with the localization of Lewy pathology present in post-mortem brains of DLB patients, with some cases even delineated as being “amygdala-predominant” (Attems et al., 2021). Overall, such pattern of cortical and limbic pSyn129 labeling, as identified in the SNCA model, is pathognomonic of α-syn pathology present in DLB subjects (Driver-Dunckley et al., 2014; Outeiro et al., 2019).

To date, there are conflicting viewpoints about the correlation between the amount of cortical Lewy body burden and gravity of cognitive symptoms (Buldyrev et al., 2000; Kövari et al., 2003). Strikingly,

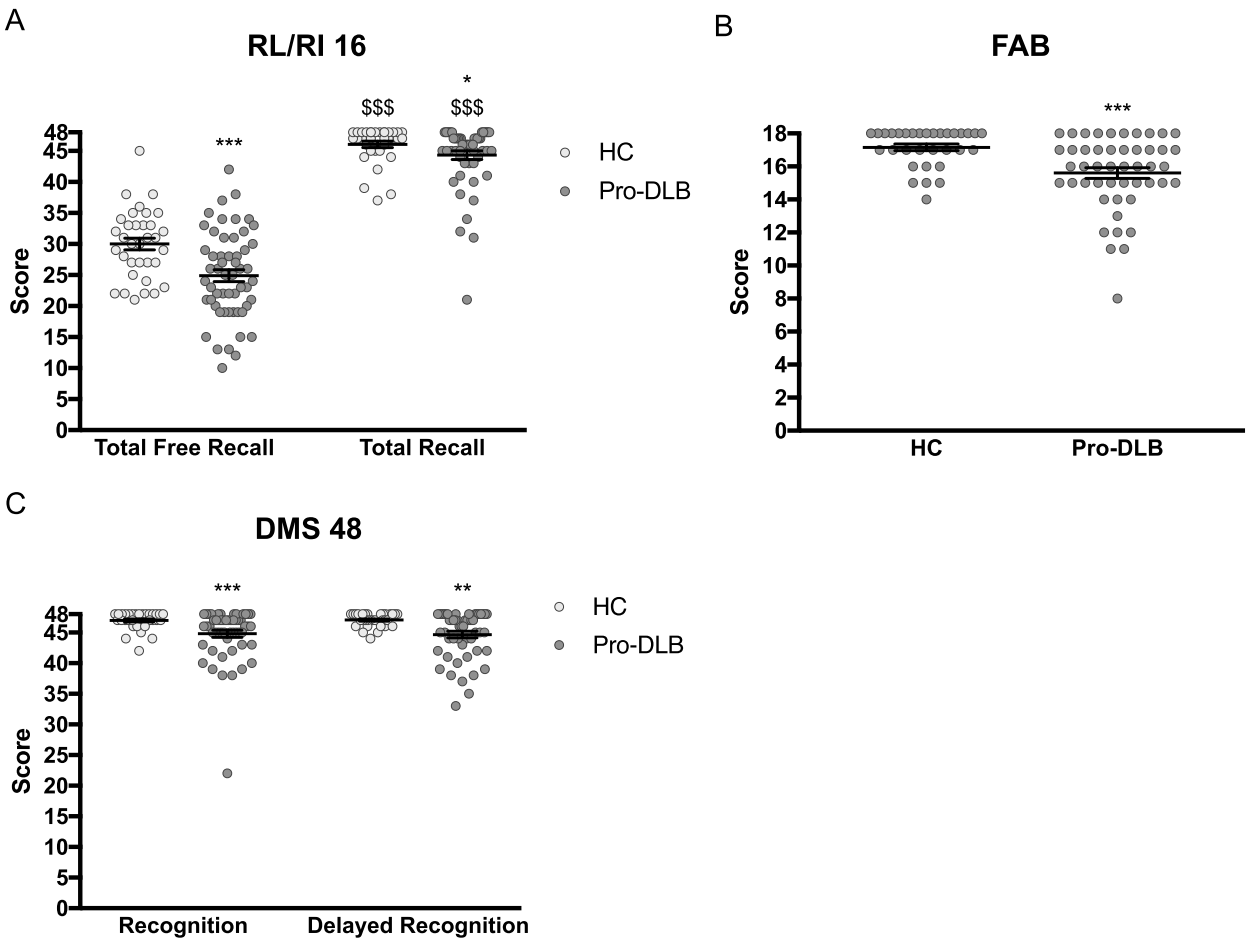

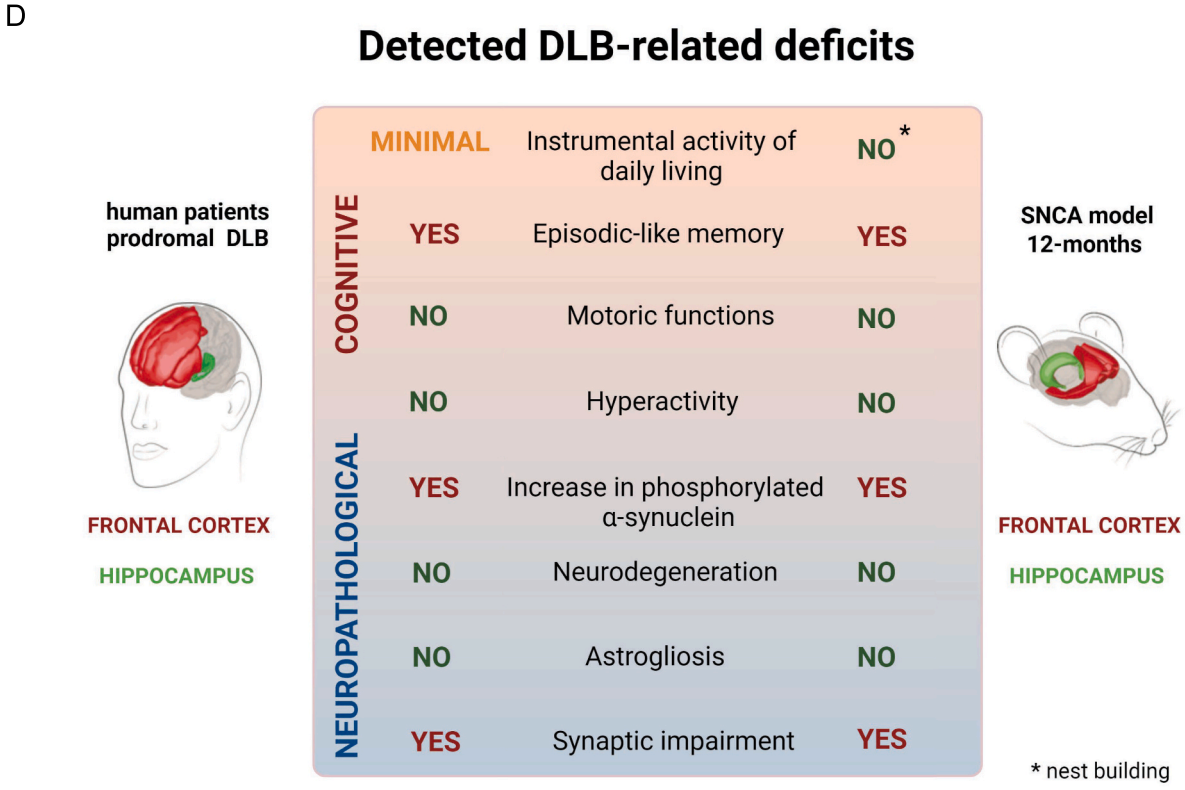

(caption on next page)

Fig. 8. Cognitive tests performed in Pro-DLB patients show frontal-related deficits. (A) The results of the (RL/RI-16) test show a more significant deficit for the total free recall than the total recall in the Pro-DLB cohort compared to healthy controls (HC) (HC, $n = 34$; Pro-DLB, $n = 55$). (B) The results of the FAB test show a significant deficit in Pro-DLB patients (HC, $n = 32$; Pro-DLB, $n = 48$) compared to HC. (C) DMS48 test shows a significant deficit of the immediate and delayed recognition for Pro-DLB patients (HC, n = 34; Pro-DLB Recognition, $n = 54$ or Pro-DLB Delayed Recognition, $n = 52$). Data are shown as mean ± SEM (* $p < 0,05$, ** $p < 0,01$, *** $p < 0,001$ compared to HC, $$$ $p < 0,001$ compared to Total Free Recall in same experimental group, Mann-Whitney). (D) Summary diagram showing the homologies described in this report between human prodromal disease and the SNCA mouse model.

although the hippocampus carries a significant burden of α-syn pathology, we did not observe additional functional deficits associated with this structure, among those we tested, such as neuroinflammation or synaptic-related protein levels. However, we observed a reduction in the CA3 layer thickness of the SNCA compared to WT mice. This finding suggests that there may be a causal link between overexpression of the human α-syn and structural impairment of the CA3 cell layer integrity, a region affected by neurodegeneration in DLB cases (Harding and Halliday, 2001). Nevertheless, it should be pointed out that the insertion of the α-syn transgene into chromosome 14 induced duplication in the *Slc4a7* gene (solute carrier family 4, sodium bicarbonate cotransporter, member 7) (Goodwin et al., 2019). This duplication results in a functional knockout (KO) in homozygous transgenic mice, hence making the heterozygous SNCA model invalidated for one copy of the *Slc4a7* gene. This sodium bicarbonate co-transporter plays an important role in intracellular pH regulation, which is crucial for neuronal excitability (Park et al., 2010). In rodents, it is observed that the Slc4a7 co-transporter is expressed in cell bodies of CA1 and CA3 neurons, as well as in proximal dendrites of the stratum lucidum or projecting foamed fibers from the granular cells of the DG (Park et al., 2010; Boedtkjer and Pedersen, 2020). Therefore, it cannot be excluded that the partial functional *Slc4a7* KO in the SNCA model actually impacts the excitability of pyramidal hippocampal neurons, and consequently decreases the thickness of the CA3 neuronal layer – indicative of structure shrinkage or neuronal loss (Kril and Halliday, 2004). Compellingly, even though both DH and FC display the same level of *Slc4a7* downregulation, in the SNCA model we did not detect substantial behavioral deficits that are usually linked to hippocampal dysfunction, while we did so for FC-dependent ones. In physiological conditions, neurons from both structures show similar levels of *Slc4a7* expression (Saunders et al., 2018), indicating that the hemiKO of the *Slc4a7* gene is not solely accountable for the FC-originating cognitive deficit present in the model.

That being said, in the SNCA mice we detected decreased protein levels of the presynaptic marker SYP, postsynaptic marker PSD95 and the presynaptic/axonal marker RAB10 in the FC exclusively. Reduction of PSD95 is commonly reported under neurodegenerative and aging conditions (Bustos et al., 2017). Lower SYP and RAB10 levels is indicative of synaptic impairment in the FC of the SNCA model. Several lines of evidence have verified a pronounced correlation between the decrease in synaptic markers with the onset of cognitive deficits (Bereczki et al., 2016; Bereczki et al., 2018). In DLB patients, it is also widely accepted that the synaptic damage precedes neurodegeneration (Schulz-Schaeffer, 2010), and albeit we did record down-regulation of synaptic markers in the FC, this was not the case for NEUN, widely used as a neuronal marker – suggesting the absence of FC neuronal loss in the model. Unlike protein, the mRNA levels of synaptic markers remained unchanged, with *Dlg4* exhibiting upregulation tendency, a possible compensatory mechanism that arose as an attempt to replenish its protein deficiency.

The inflammatory profile of DLB patients remains poorly elucidated. Studies to date tend to show greater involvement and manifestation of neuroinflammation in the prodromal phase of the disease, which is subsequently inversely proportional to cognitive decline (Amin et al., 2022). In this study, we found transcription levels of inflammatory markers upregulated in the FC - indicating that this region is an inflammatory milieu and as such a fertile ground for functional impairments. Among the upregulated genes is the one coding for pro-inflammatory IL1β, that is the most consistently and noticeably raised cytokine in prodromal DLB (Amin et al., 2022), as well as TNFα, shown to be secreted by α-syn exposed microglia in vitro (Daniele et al., 2015) and upregulated in brains of α-syn transgenic mice (Iba et al., 2020). Moreover, our qPCR analysis uncovered slightly elevated transcription of the *Ifngr2* gene, which is again in accordance with data from Iba et al. (2020) that could be indicative of peripheral CD3+ T-cells infiltration in brains of SNCA mice, as observed in the aforementioned study. This point, however, remains undocumented and should be assessed in future research, as it would provide novel insights into the role of peripheral immunity in DLB-development. Notably, transcription levels of the *Iba1* gene, a pan-microglial marker, were downregulated in the FC of SNCA mice, coincidentally with upregulation of *Cd68,* that is a marker of activated phagocytic microglia (Lemstra et al., 2007). This pattern of gene expression is characteristic of disease associated microglia (DAM), a concept linked to neurodegeneration (Lier et al., 2021), and has been detected in brains of DLB patients (Streit and Xue, 2016), as well as in αSyn-APOE4 transgenic animals (Zhao et al., 2020). However, we did not find any significant difference at the level of the IBA1 protein in the mPFC, nor in the DH at this age, but a tendency of decreased IBA1 levels were noted only in the mPFC, consistent with the decrease in mRNA expression observed in this structure, suggesting IBA1 down-regulation may occur at later stages. The involvement of neuroinflammation in DLB development and progression remains elusive, though the results obtained in this study are in accordance with the inflammatory environment assigned to DLB patients. Even the lack of change in mRNA and protein expression of the astrocytic activation marker GFAP in the SNCA model is consistent with the absence of reactive gliosis in synucleinopathies patients, contrary to AD ones (Mirza et al., 2000). Finally, Zhao et al. (2020) reported no correlation between pS129-positive α-synuclein and GFAP or IBA1 immunoreactivities in both DLB brains with minimal amyloid pathology and in mouse models, indicating that glial activation is not associated with α-synuclein pathology.

5. Conclusion

Overall, the behavioral, anatomopathological and molecular characterization of the SNCA model conducted throughout this study uncovered a prevalent FC-related deficit manifested by the presence of α-syn pathology, inflammation and dysregulation of synaptic plasticity underscored by impaired cognitive functions. Even though there was substantial α-syn neuropathology detected in the DH as well, there were no hippocampal-related cognitive or molecular deficits accompanying it at this stage. Interestingly, this pattern of FC-emanating cognitive deficiency with preserved DH function is observed in prodromal DLB patients, making this model a practical tool, and to our knowledge the first one, for conducting research on early stages of DLB.

Funding

This work was supported by funding from the University of Strasbourg, Centre National de la Recherche Scientifique (CNRS, UMR7364), the Union France Alzheimer (Association France Alzheimer maladies apparentées AAP SM 2017 #1664), Association des Aidants et Malades à Corps de Lewy (A2MCL, 2022), IDEX Recherche Exploratoire (2022) and the Interdisciplinary Thematic Institute NeuroStra, as part of the ITI 2021–2028 program of the University of Strasbourg, CNRS and Inserm supported by IdEx Unistra (ANR-10-IDEX-0002). ES and IG were supported by a doctoral fellowship from the "Ministère de la Recherche"

(France). IG was also supported by an end of thesis grant obtained from the Foundation “Vaincre Alzheimer” (France). AlphaLewyMA cohort was funded by PHRC interregional (N° IDRCB 2012-A00992–41).

Disclosures

The authors have nothing to disclose.

CRediT authorship contribution statement

Estelle Schueller: Writing – review & editing, Writing – original draft, Visualization, Methodology, Investigation, Formal analysis, Conceptualization. **Iris Grgurina:** Writing – review & editing, Writing – original draft, Visualization, Methodology, Investigation, Formal analysis. **Brigitte Cosquer:** Methodology, Investigation. **Elodie Panzer:** Methodology, Visualization, Investigation. **Noémie Penaud:** Methodology, Visualization, Investigation. **Anne Pereira de Vasconcelos:** Methodology, Visualization. **Aline Stéphan:** Methodology. **Karine Merienne:** Methodology. **Jean-Christophe Cassel:** Writing – review & editing. **Chantal Mathis:** Methodology, Writing – review & editing. **Frédéric Blanc:** Writing – review & editing, Visualization, Validation, Supervision, Methodology, Funding acquisition, Conceptualization. **Olivier Bousiges:** Writing – review & editing, Writing – original draft, Visualization, Validation, Supervision, Methodology, Investigation, Formal analysis, Conceptualization. **Anne-Laurence Boutillier:** Writing – review & editing, Writing – original draft, Visualization, Supervision, Resources, Project administration, Methodology, Investigation, Funding acquisition, Formal analysis, Conceptualization.

Declaration of competing interest

The authors declare that they have no known competing financial interests or personal relationships that could have appeared to influence the work reported in this paper.

Data availability

Data will be made available on request.

Acknowledgments

We thank Olivier Bildstein, Onwukanjo-Daniel Egesi, George Edomwonyi (UMR 7364, Strasbourg) for animal care, Carole Reinwalt and Aminé Isik for generating and genotyping the Thy1-hSNCA mice. We thank Kelly Louis and Charles Dupuy for performing some of the WB experiments, Isabel Paiva for qPCR dosage of the *Slc4a7*, *hSNCA* and *mSNCA* genes, Léna Rugiero for performing TH labeling in the substantia nigra and microscopy acquisitions, and Johanne Gambi for additional microscopy acquisitions. We warmly thank patient’s associations which help us to pursue this work: Alsace Alzheimer 67; Association des Aidants et Malades à Corps de Lewy (A2MCL).

Appendix A. Supplementary data

Supplementary data to this article can be found online at https://doi.org/10.1016/j.nbd.2024.106676.

References

Amin, J., Erskine, D., Donaghy, P.C., Surendranathan, A., Swann, P., Kunicki, A.P., et al., 2022. Inflammation in dementia with Lewy bodies. Neurobiol. Dis. 168, 105698.
Attems, J., Toledo, J.B., Walker, L., Gelpi, E., Gentleman, S., Halliday, G., et al., 2021. Neuropathological consensus criteria for the evaluation of Lewy pathology in post-mortem brains: a multi-Centre study. Acta Neuropathol. 141 (2), 159–172.
Barbeau, E., Didic, M., Tramoni, E., Felician, O., Joubert, S., Sontheimer, A., et al., 2004a. Evaluation of visual recognition memory in MCI patients. Neurologys 62 (8), 1317–1322.
Barbeau, E., Sontheimer, A., Joubert, S., Didic, M., Felician, O., Tramoni, E., et al., 2004b. Le cortex périrhinal chez l’homme [the human perirhinal cortex]. Rev. Neurol. (Paris) 160 (4 Pt 1), 401–411.
Barker, G.R., Bird, F., Alexander, V., Warburton, E.C., 2007. Recognition memory for objects, place, and temporal order: a disconnection analysis of the role of the medial prefrontal cortex and perirhinal cortex. J. Neurosci. 27 (11), 2948–2957.
Bereczki, E., Francis, P.T., Howlett, D., Pereira, J.B., Höglund, K., Bogstedt, A., et al., 2016. Synaptic proteins predict cognitive decline in Alzheimer’s disease and Lewy body dementia. Alzheimers Dement. 12 (11), 1149–1158.
Bereczki, E., Branca, R.M., Francis, P.T., Pereira, J.B., Baek, J.H., Hortobágyi, T., et al., 2018. Synaptic markers of cognitive decline in neurodegenerative diseases: a proteomic approach [published correction appears in brain. 2019 Jun 1;142(6): e24]. Brain 141 (2), 582–595.
Blanc, F., Colloby, S.J., Philippi, N., de Pétigny, X., Jung, B., Demuynck, C., et al., 2015. Cortical thickness in dementia with Lewy bodies and Alzheimer’s disease: a comparison of prodromal and dementia stages. PLoS One 10 (6), e0127396.
Blanc, F., Colloby, S.J., Cretin, B., de Sousa, P.L., Demuynck, C., O’Brien, J.T., et al., 2016. Grey matter atrophy in prodromal stage of dementia with Lewy bodies and Alzheimer’s disease. Alzheimers Res. Ther. 8, 31.
Boedtkjer, E., Pedersen, S.F., 2020. The acidic tumor microenvironment as a Driver of Cancer. Annu. Rev. Physiol. 82, 103–126.
Brown, M.W., Aggleton, J.P., 2001. Recognition memory: what are the roles of the perirhinal cortex and hippocampus? Nat. Rev. Neurosci. 2 (1), 51–61.
Buldyrev, S.V., Cruz, L., Gomez-Isla, T., Gomez-Tortosa, E., Havlin, S., Le, R., et al., 2000. Description of microcolumnar ensembles in association cortex and their disruption in Alzheimer and Lewy body dementias. Proc. Natl. Acad. Sci. USA 97 (10), 5039–5043.
Bustos, F.J., Ampuero, E., Jury, N., Aguilar, R., Falahi, F., Toledo, J., et al., 2017. Epigenetic editing of the Dlg4/PSD95 gene improves cognition in aged and Alzheimer’s disease mice. Brain 140 (12), 3252–3268.
Chao, O.Y., Huston, J.P., Nikolaus, S., de Souza Silva, M.A., 2016. Concurrent assessment of memory for object and place: evidence for different preferential importance of perirhinal cortex and hippocampus and for promnestic effect of a neurokinin-3 R agonist. Neurobiol. Learn. Mem. 130, 149–158.
Chatterjee, S., Cassel, R., Schneider-Anthony, A., Merienne, K., Cosquer, B., Tzeplaeff, L., et al., 2018. Reinstating plasticity and memory in a tauopathy mouse model with an acetyltransferase activator. EMBO Mol. Med. 10 (11), e8587.
Chiba, Y., Fujishiro, H., Iseki, E., Ota, K., Kasanuki, K., Hirayasu, Y., et al., 2012. Retrospective survey of prodromal symptoms in dementia with Lewy bodies: comparison with Alzheimer’s disease. Dement. Geriatr. Cogn. Disord. 33 (4), 273–281.
Crabtree, D.M., Zhang, J., 2012. Genetically engineered mouse models of Parkinson’s disease. Brain Res. Bull. 88 (1), 13–32.
Daniele, S.G., Béraud, D., Davenport, C., Cheng, K., Yin, H., Maguire-Zeiss, K.A., 2015. Activation of MyD88-dependent TLR1/2 signaling by misfolded α-synuclein, a protein linked to neurodegenerative disorders. Sci. Signal. 8 (376), ra45.
Delli Pizzi, S., Franciotti, R., Bubbico, G., Thomas, A., Onofrj, M., Bonanni, L., 2016. Atrophy of hippocampal subfields and adjacent extrahippocampal structures in dementia with Lewy bodies and Alzheimer’s disease. Neurobiol. Aging 40, 103–109.
Donaghy, P.C., McKeith, I.G., 2014. The clinical characteristics of dementia with Lewy bodies and a consideration of prodromal diagnosis. Alzheimers Res. Ther. 6 (4), 46.
Doty, R.L., 2012. Olfaction in Parkinson’s disease and related disorders. Neurobiol. Dis. 46 (3), 527–552.
Driver-Dunckley, E., Adler, C.H., Hentz, J.G., Dugger, B.N., Shill, H.A., Caviness, J.N., et al., 2014. Olfactory dysfunction in incidental Lewy body disease and Parkinson’s disease. Parkinsonism Relat. Disord. 20 (11), 1260–1262.
Dubois, B., Slachevsky, A., Litvan, I., Pillon, B., 2000. The FAB: a frontal assessment battery at bedside. Neurology 55 (11), 1621–1626.
Fenelon, G., Soulas, T., Zenasni, F., Cleret de Langavant, L., 2010. The changing face of Parkinson’s disease-associated psychosis: a cross-sectional study based on the new NINDS-NIMH criteria. Mov. Disord. 25 (6), 763–766.
Ferman, T.J., Smith, G.E., Boeve, B.F., Ivnik, R.J., Petersen, R.C., Knopman, D., et al., 2004. DLB fluctuations: specific features that reliably differentiate DLB from AD and normal aging. Neurology 62 (2), 181–187.
Fleming, S.M., Ekhator, O.R., Ghisays, V., 2013. Assessment of sensorimotor function in mouse models of Parkinson’s disease. J. Vis. Exp. 76, 50303.
Fullard, M.E., Morley, J.F., Duda, J.E., 2017. Olfactory dysfunction as an early biomarker in Parkinson’s disease. Neurosci. Bull. 33 (5), 515–525.
Gaskill, B.N., Karas, A.Z., Garner, J.P., Pritchett-Corning, K.R., 2013. Nest building as an indicator of health and welfare in laboratory mice. J. Vis. Exp. 82, 51012.
Gjerstad, M.D., Boeve, B., Wentzel-Larsen, T., Aarsland, D., Larsen, J.P., 2008. Occurrence and clinical correlates of REM sleep behaviour disorder in patients with Parkinson’s disease over time. J. Neurol. Neurosurg. Psychiatry 79 (4), 387–391.
Goodwin, L.O., Splinter, E., Davis, T.L., Urban, R., He, H., Braun, R., et al., 2019. Large-scale discovery of mouse transgenic integration sites reveals frequent structural variation and insertional mutagenesis. Genome Res. 29 (3), 494–505.
Grober, E., Sanders, A.E., Hall, C., Lipton, R.B., 2010. Free and cued selective reminding identifies very mild dementia in primary care. Alzheimer Dis. Assoc. Disord. 24 (3), 284–290.
Harding, A.J., Halliday, G.M., 2001. Cortical Lewy body pathology in the diagnosis of dementia. Acta Neuropathol. 102 (4), 355–363.
Hatami, A., Chesselet, M.F., 2015. Transgenic rodent models to study alpha-synuclein pathogenesis, with a focus on cognitive deficits. Curr. Top. Behav. Neurosci. 22, 303–330.

Iba, M., Kim, C., Sallin, M., Kwon, S., Verma, A., Overk, C., et al., 2020. Neuroinflammation is associated with infiltration of T cells in Lewy body disease and α-synuclein transgenic models. J. Neuroinflammation 17 (1), 214.
Ising, C., Venegas, C., Zhang, S., et al., 2019. NLRP3 inflammasome activation drives tau pathology. Nature 575, 669–673.
Jellinger, K.A., 2019. Is Braak staging valid for all types of Parkinson's disease? J. Neural Transm. (Vienna) 126 (4), 423–431.
Jirkof, P., 2014. Burrowing and nest building behavior as indicators of well-being in mice. J. Neurosci. Methods 234, 139–146.
Kayyal, H., Chandran, S.K., Yiannakas, A., Gould, N., Khamaisy, M., Rosenblum, K., 2021. Insula to mPFC reciprocal connectivity differentially underlies novel taste neophobic response and learning in mice. Elife 10, e66686.
Kövari, E., Gold, G., Herrmann, F.R., Canuto, A., Hof, P.R., Bouras, C., et al., 2003. Lewy body densities in the entorhinal and anterior cingulate cortex predict cognitive deficits in Parkinson's disease. Acta Neuropathol. 106 (1), 83–88.
Kril, J.J., Halliday, G.M., 2004. Clinicopathological staging of frontotemporal dementia severity: correlation with regional atrophy. Dement. Geriatr. Cogn. Disord. 17 (4), 311–315.
Lemstra, A.W., Groen in't Woud, J.C., Hoozemans, J.J., van Haastert, E.S., Rozemuller, A.J., Eikelenboom, P., et al., 2007. Microglia activation in sepsis: a case-control study. J. Neuroinflammation 4, 4.
Lier, J., Streit, W.J., Bechmann, I., 2021. Beyond activation: characterizing microglial functional phenotypes. Cells 10 (9), 2236.
Lim, Y., Kehm, V.M., Lee, E.B., Soper, J.H., Li, C., Trojanowski, J., et al., 2011. α-Syn suppression reverses synaptic and memory defects in a mouse model of dementia with Lewy bodies. J. Neurosci. 31 (27), 10076–10087.
Livak, K.J., Schmittgen, T.D., 2001. Analysis of relative gene expression data using real-time quantitative PCR and the 2(-Delta Delta C(T)) method. Methods 25 (4), 402–408.
Lopez, J., Herbeaux, K., Cosquer, B., Engeln, M., Muller, C., Lazarus, C., Kelche, C., Bontempi, B., Cassel, J.C., de Vasconcelos, A.P., 2012. Context-dependent modulation of hippocampal and cortical recruitment during remote spatial memory retrieval. Hippocampus 22 (4), 827–841.
Maviel, T., Durkin, T.P., Menzaghi, F., Bontempi, B., 2004. Sites of neocortical reorganization critical for remote spatial memory. Science 305 (5680), 96–99.
McKeith, I.G., Galasko, D., Kosaka, K., Perry, E.K., Dickson, D.W., Hansen, L.A., et al., 1996. Consensus guidelines for the clinical and pathologic diagnosis of dementia with Lewy bodies (DLB): report of the consortium on DLB international workshop. Neurology 47 (5), 1113–1124.
McKeith, I.G., Ferman, T.J., Thomas, A.J., Blanc, F., Boeve, B.F., Fujishiro, H., et al., 2020. Research criteria for the diagnosis of prodromal dementia with Lewy bodies. Neurology 94 (17), 743–755.
Meeus, B., Verstraeten, A., Crosiers, D., Engelborghs, S., Van den Broeck, M., Mattheijssens, M., Peeters, K., Corsmit, E., Elinck, E., Pickut, B., Vandenberghe, R., Cras, P., De Deyn, P.P., Van Broeckhoven, C., Theuns, J., 2012. DLB and PDD: a role for mutations in dementia and Parkinson disease genes? Neurobiol. Aging 33 (3), 629.e5–629.e18.
Mirza, B., Hadberg, H., Thomsen, P., Moos, T., 2000. The absence of reactive astrocytosis is indicative of a unique inflammatory process in Parkinson's disease. Neuroscience 95 (2), 425–432.
Moraga-Amaro, R., Cortés-Rojas, A., Simon, F., Stehberg, J., 2014. Role of the insular cortex in taste familiarity. Neurobiol. Learn. Mem. 109, 37–45.
Nelson, P.T., Schmitt, F.A., Jicha, G.A., Kryscio, R.J., Abner, E.L., Smith, C.D., et al., 2010. Association between male gender and cortical Lewy body pathology in large autopsy series. J. Neurol. 257 (11), 1875–1881.
Oppedal, K., Ferreira, D., Cavallin, L., Lemstra, A.W., Ten Kate, M., Padovani, A., Rektorova, I., Bonanni, L., Wahlund, L.O., Engedal, K., Nobili, F., Kramberger, M., Taylor, J.P., Hort, J., Snædal, J., Blanc, F., Walker, Z., Antonini, A., Westman, E., Aarsland, D., Alzheimer's Disease Neuroimaging Initiative, 2019. A signature pattern of cortical atrophy in dementia with Lewy bodies: a study on 333 patients from the European DLB consortium. Alzheimers Dement. 15 (3), 400–409.
Outeiro, T.F., Koss, D.J., Erskine, D., Walker, L., Kurzawa-Akanbi, M., Burn, D., et al., 2019. Dementia with Lewy bodies: an update and outlook. Mol. Neurodegener. 14 (1), 5.
Ouyang, Y., 2011. Direct Data Submission 2011/07/19. MGI Direct Data Submission.
Park, H.J., Rajbhandari, I., Yang, H.S., Lee, S., Cucoranu, D., Cooper, D.S., et al., 2010. Neuronal expression of sodium/bicarbonate cotransporter NBCn1 (SLC4A7) and its response to chronic metabolic acidosis. Am. J. Phys. Cell Phys. 298 (5), C1018–C1028.
Perez, F., Helmer, C., Dartigues, J.F., Auriacombe, S., Tison, F., 2010. A 15-year population-based cohort study of the incidence of Parkinson's disease and dementia with Lewy bodies in an elderly French cohort. J. Neurol. Neurosurg. Psychiatry 81 (7), 742–746.
Philippi, N., Noblet, V., Duron, E., Cretin, B., Boully, C., Wisniewski, I., et al., 2016. Exploring anterograde memory: a volumetric MRI study in patients with mild cognitive impairment. Alzheimers Res. Ther. 8 (1), 26.
Roquet, D., Noblet, V., Anthony, P., Philippi, N., Demuynck, C., Cretin, B., et al., 2017. Insular atrophy at the prodromal stage of dementia with Lewy bodies: a VBM DARTEL study. Sci. Rep. 7 (1), 9437.
Rullier, L., Matharan, F., Barbeau, E.J., Mokri, H., Dartigues, J.F., Pérès, K., et al., 2014. Test du DMS 48 : normes chez les sujets âgés et propriétés de détection de la maladie d'Alzheimer dans la cohorte AMI [The DMS 48: norms and diagnostic proprieties for Alzheimer's disease in elderly population from the AMI cohort study]. Geriatr. Psychol. Neuropsychiatr. Vieil. 12 (3), 321–330.
Saunders, A., Macosko, E.Z., Wysoker, A., Goldman, M., Krienen, F.M., de Rivera, H., et al., 2018. Molecular diversity and specializations among the cells of the adult mouse brain. Cell 174 (4), 1015–1030.e16.
Savica, R., Grossardt, B.R., Bower, J.H., Boeve, B.F., Ahlskog, J.E., Rocca, W.A., 2013. Incidence of dementia with Lewy bodies and Parkinson disease dementia. JAMA Neurol. 70 (11), 1396–1402.
Schulz-Schaeffer, W.J., 2010. The synaptic pathology of alpha-synuclein aggregation in dementia with Lewy bodies, Parkinson's disease and Parkinson's disease dementia. Acta Neuropathol. 120 (2), 131–143.
Singleton, A.B., Farrer, M., Johnson, J., Singleton, A., Hague, S., Kachergus, J., Hulihan, M., Peuralinna, T., Dutra, A., Nussbaum, R., Lincoln, S., Crawley, A., Hanson, M., Maraganore, D., Adler, C., Cookson, M.R., Muenter, M., Baptista, M., Miller, D., Blancato, J., Hardy, J., Gwinn-Hardy, K., 2003. Alpha-Synuclein locus triplication causes Parkinson's disease. Science 302 (5646), 841.
Spillantini, M.G., Schmidt, M.L., Lee, V.M., Trojanowski, J.Q., Jakes, R., Goedert, M., 1997. Alpha-synuclein in Lewy bodies. Nature 388 (6645), 839–840.
Streit, W.J., Xue, Q.S., 2016. Microglia in dementia with Lewy bodies. Brain Behav. Immun. 55, 191–201.
Swank, M.W., Sweatt, J.D., 2001. Increased histone acetyltransferase and lysine acetyltransferase activity and biphasic activation of the ERK/RSK cascade in insular cortex during novel taste learning. J. Neurosci. 21 (10), 3383–3391.
Thomas, A.J., Hamilton, C.A., Barker, S., Durcan, R., Lawley, S., Barnett, N., et al., 2022. Olfactory impairment in mild cognitive impairment with Lewy bodies and Alzheimer's disease. Int. Psychogeriatr. 34 (6), 585–592.
Van der Linden, M., Coyette, F., Poitrenaud, J., Kalafat, M., Calacis, F., Wyns, C., Adam, S., Membres du GREMEM, et al., 2004. L'épreuve de rappel libre/rappelindicé à 16 items (RL/RI-16). In: Van der Liden, M., Adam, S., Agniel, A., BaissetMouly, C., et al. (Eds.), L'évaluation des troubles de la mémoire : Présentation de quatre tests demémoire épisodique (avec leur étalonnage). Marseille, Solal.
Yanai, S., Endo, S., 2021. Functional aging in male C57BL/6J mice across the life-span: a systematic behavioral analysis of motor, emotional, and memory function to define an aging phenotype. Front. Aging Neurosci. 13, 697621.
Yang, M., Crawley, J.N., 2009. Simple behavioral assessment of mouse olfaction. Curr Protoc Neurosci. Chapter 8: Unit 8.24.1-8.24.12.
Yiannakas, A., Rosenblum, K., 2017. The insula and taste learning. Front. Mol. Neurosci. 10, 335 (Published 2017 Nov 3).
Zaccai, J., McCracken, C., Brayne, C., 2005. A systematic review of prevalence and incidence studies of dementia with Lewy bodies. Age Ageing 34 (6), 561–566.
Zhao, N., Attrebi, O.N., Ren, Y., Qiao, W., Sonustun, B., Martens, Y.A., et al., 2020. APOE4 exacerbates α-synuclein pathology and related toxicity independent of amyloid. Sci. Transl. Med. 12 (529), eaay1809.
Zhou, W., Milder, J.B., Freed, C.R., 2008. Transgenic mice overexpressing tyrosine-to-cysteine mutant human alpha-synuclein: a progressive neurodegenerative model of diffuse Lewy body disease. J. Biol. Chem. 283 (15), 9863–9870.